Covenant Journal of Physical & Life Sciences

Vol. 3 No. 1, June 2015

A Publication of Covenant University

Editor-in-Chief: Prof. Dilip De
E-mail: dlpd770@gmail.com

Managing Editor: Edwin O. Agbaike
E-mail: edwin.agbaike@covenantuniversity.edu.ng

Htt//journals.covenantuniversity.edu.ng/cjpl/

© 2013, Covenant University Journals.

All rights reserved. No part of this publication may be reproduced, stored in a retrieval system or transmitted in any form or by any meams, electronic, electrostatic, magnetic tape, mechanical, photocopying, recording or otherwise, without the prior written permission of the publisher.

It is a condition of publication in this journal that manuscripts have not been published or submitted for publication and will not be submitted or published elsewhere.

Upon the acceptance of articles to be published in this journal,the author(s) are required to transfer copyright of the article to the publisher.

ISSN - Print: 2354 – 3574
- Electronics: 2354 – 3485

Published by Covenant University Journals,

KM. 10 Idiroko Road, Canaan Land,
Ota, Ogun State, Nigeria

Printed by Covenant University Press.

Contents

A Note on the Minimax Distribution

Oguntunde, P. E[1], Adejumo, A. O[2]

[1]Department of Mathematics,
Covenant University, Ota, Ogun State, Nigeria

[2]Department of Statistics,
University of Ilorin, Kwara State, Nigeria

***Abstract*:** We introduce a one parameter probability model bounded on (0, 1) support called *One Parameter Minimax distribution* which is a special case of both the Kumaraswamy distribution and Beta distribution. Its statistical properties are systematically explored; we provide explicit expressions for its moments, quantile function, reliability function and failure rate. The method of maximum likelihood estimation was used in estimating its parameter. The proposed model can be used to model data sets with increasing failure rates.

Keywords: Beta distribution, Increasing failure rate, Kumaraswamy distribution, Minimax distribution.

1.0 Introduction

According to [4] and [6], "Despite the many alternatives and generalizations, it remains fair to say that the beta distribution provides the premier family of continuous distributions on bounded support (which is taken to be (0, 1))". Let X denote a non-negative continuous random variable that follows a beta distribution with parameters 'a' and 'b', we write; $X \sim Beta(a,b)$, the probability density function is given by;

$$f(x) = \frac{\Gamma(a+b)}{\Gamma(a)\Gamma(b)} x^{a-1}(1-x)^{b-1};$$

$$x \in (0,1) \quad (1)$$

Where $a,b>0$ are shape parameters

Besides lot of other attractive properties, the shape of beta densities could be unimodal, uniantimodal, constant, increasing or decreasing depending on the values of parameters 'a' and 'b' relative to 1 ; See [1] for details. It is good to note that the cumulative density function of the beta distribution involves an incomplete beta function; this makes the distribution not to be very tractable.

[5] introduced the Kumaraswamy distribution and many authors have explored some of the properties of this distribution. Noticeably is the work of [2] who described the distribution as a Minimax distribution sharing many desirable properties with the beta distribution. The Minimax distribution has been

described as a viable alternative to the beta distribution and its basic properties reflects that it is more tractable compared to the beta distribution.

For a random variable X having Minimax distribution with parameters 'a' and 'b', the probability density function (pdf) is given by;

$$f(x) = abx^{a-1}\left(1-x^{a}\right)^{b-1} \; ; \; x \in (0,1) \quad (2)$$

The corresponding cumulative density function (cdf) is given by;

$$F(x) = 1-\left(1-x^{a}\right)^{b} \quad ; \quad x \in (0,1) \quad (3)$$

Where $a, b > 0$ are shape parameters

We refer readers to [7] and [8] for some details on the Minimax distribution.

This article seeks to extend the notable work of [3] by exploring a special case of both the beta distribution and the Minimax distribution when we assume one of the shape parameters 'a' to equal 1, we also investigate some basic statistical properties of the resulting model.

The rest of this article is organized as follows; section two discusses how the new model was derived including derivations of some of its basic properties, section three discusses the estimation of the model parameter using the method of maximum likelihood estimation, followed by a concluding remark.

2.0 The Proposed Model

Substituting $a = 1$ in both Equation (1) and (2) gives the pdf of the proposed model to be;

$$f(x) = b(1-x)^{b-1} \quad ; \quad x \in (0,1) \quad (4)$$

Thus, we easily derive its cdf to give;

$$F(x) = 1-(1-x)^{b} \quad ; \quad x \in (0,1) \quad (5)$$

Where $b > 0$ is a shape parameter

2.1 The new model is a valid probability density function

To proof that the model in Equation (4) is a valid pdf, we show that integrating Equation (4) with respect to x from 0 to 1 equals 1. That is,

$$\int_0^1 b(1-x)^{b-1}dx = 1$$

Let $u = (1-x)$; then, $dx = -du$

Therefore,

$$\int_0^1 b(1-x)^{b-1}dx = -b\int_0^1 u^{b-1}du$$

After simple calculations,

$$\int_0^1 b(1-x)^{b-1}dx = 1$$

This completes the proof.

We also provide graphical representations of the pdf of the model and at various values of parameter 'b'. For brevity purpose, we present plots for the pdf at '$b = 1$', '$b = 4$' and at '$b = 20$' in Figure 1, 2 and 3 respectively.

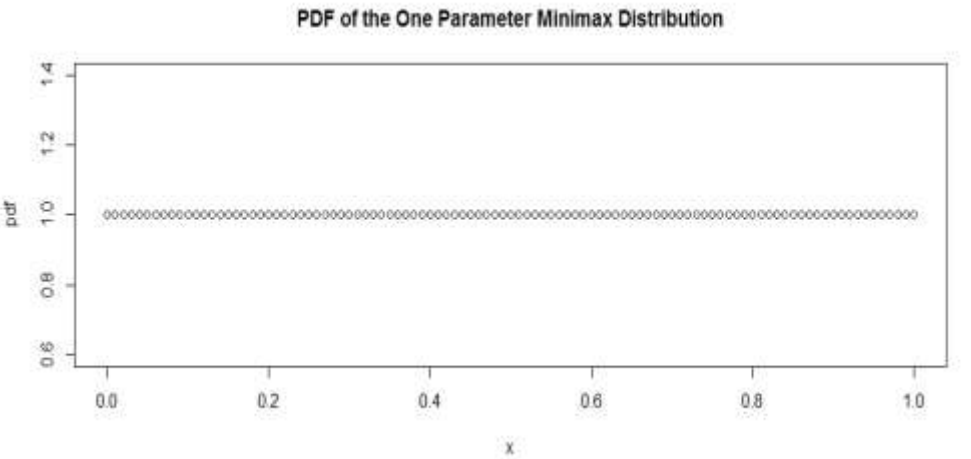

Fig. 1: The pdf of the proposed model when parameter $b = 1$

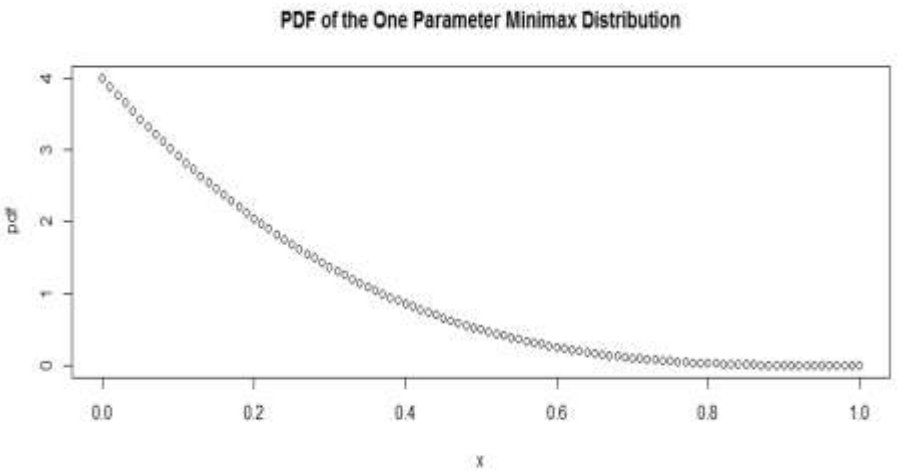

Fig. 2: The pdf of the proposed model when parameter $b = 4$

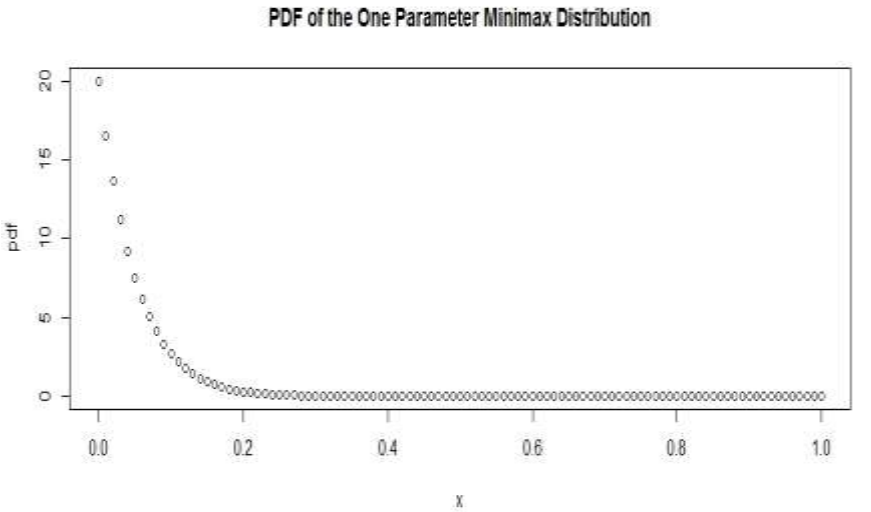

Fig. 3: The pdf of the proposed model when parameter $b = 20$

We observe in Figure 1 that the shape of the model could be "constant" and both plots in Figure 2 and 3 indicate that as the value of 'x' increases, the curve decreases. Hence, we can also say the shape of the model could be "decreasing". A plot for the cdf of the model is as shown in Figure 4;

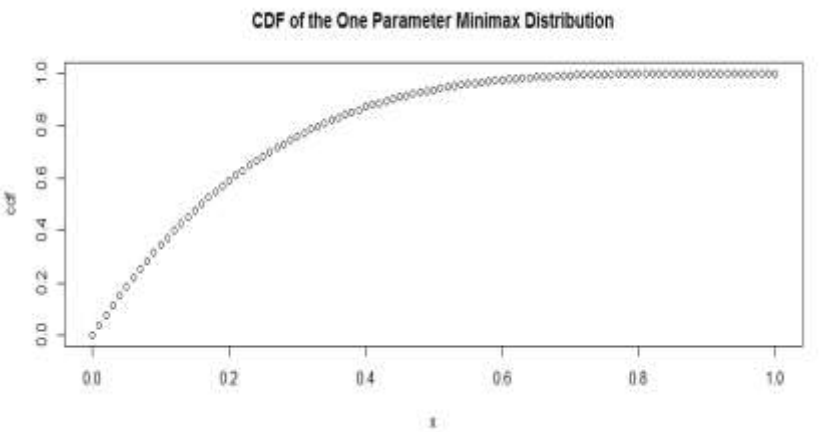

Fig. 4: The cdf of the model when parameter $'b = 4'$

2.2 Some properties of the new model

In this section, we provide some desirable properties of the new model, beginning with its moments.

2.2.1 Moments

The rth moment for a random variable X denoted by μ_r is given by;

$$\mu_r = E\left[X^r \right]$$

Hence, the rth moment for the new model in Equation (4) is given by;

$$\mu_r = b\int_0^1 x^r \left(1-x\right)^{b-1} dx$$

After simple calculations, we obtain the rth moment as;

$$\mu_r = bB\left(r+1,b\right) \qquad (6)$$

We can simply re-write Equation (6) as;

$$\mu_r = \frac{\Gamma\left(r+1\right)\Gamma\left(b+1\right)}{\Gamma\left(b+r+1\right)} \qquad (7)$$

Note that, $\Gamma\left(k\right) = \left(k-1\right)!$

where; $k > 0$ is an arbitrary constant. The mean, μ_1 is easily gotten as;

$$Mean = \frac{1}{b+1} \qquad (8)$$

The variance is given by;

$$Var\left(X\right) = bB\left(3,b\right) - \left[bB\left(2,b\right)\right]^2$$

$$Var\left(X\right) = \frac{b}{\left(b+1\right)^2\left(b+2\right)} \qquad (9)$$

With the expression given in Equation (6), other higher-order moments can be obtained.

2.2.2 The Quantile Function and Median

The quantile function Q is an alternative to the pdf as it is a way of prescribing a probability distribution and it can be derived as the inverse of the cdf. With this understanding, we give the expression for the quantile function of the new model as;

$$Q\left(u\right) = 1-\left(1-u\right)^{1/b} \qquad (10)$$

The median of the model can be obtained by substituting $u = 0.5$ into Equation (10). Therefore, we have;

$$Median = 1-\left(1-0.5\right)^{1/b}$$

This can be simplified to give;

$$Median = 1-\left(0.5\right)^{1/b} \qquad (11)$$

For simulation purposes, random variables from the new model can be obtained using the expression;

$$X = 1-\left(1-u\right)^{1/b} \qquad (12)$$

where $U \sim Uniform\left(0,1\right)$

2.2.3 Reliability Analysis

The reliability (survival function) for the model in Equation (4) is derived by;

$$S\left(x\right) = 1-F\left(x\right)$$

$$= 1-\left[1-\left(1-x\right)^b\right]$$

$$S\left(x\right) = \left(1-x\right)^b \qquad (13)$$

The corresponding plot for the survival function of the model is as shown in Figure 5;

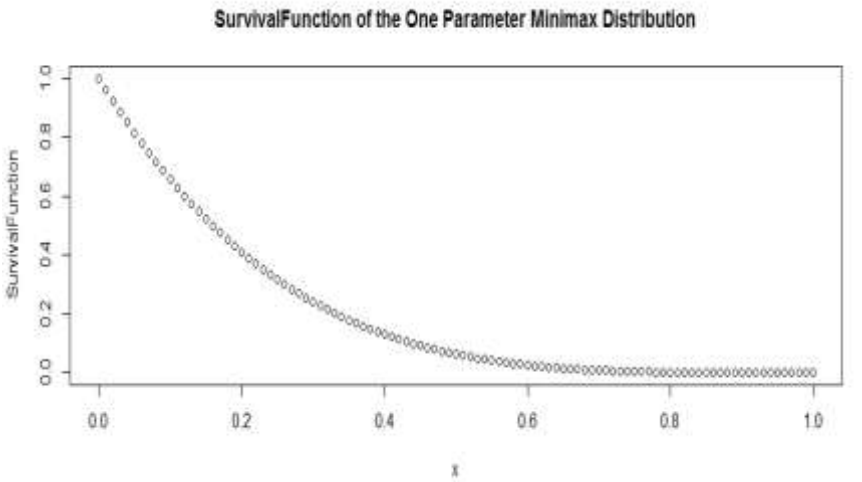

Fig. 5: The Survival Function of the model when parameter $'b=4'$

The probability that a system having age $'x'$ units of time will survive up to $'x+t'$ units of time for $x>0, b>0$ is given by;

$$S(t\mid x)=\frac{S(x+t)}{S(x)}$$

$$S(t\mid x)=\frac{\left(1-\left(x+t\right)\right)^{b}}{\left(1-x\right)^{b}} \qquad (14)$$

The corresponding hazard function is thus given by;

$$h(x)=\frac{f(x)}{1-F(x)}$$

$$=\frac{b\left(1-x\right)^{b-1}}{1-\left[1-\left(1-x\right)^{b}\right]}$$

$$h(x)=\frac{b}{\left(1-x\right)} \qquad (15)$$

We obtain plots for the hazard function of the model at various parameter values but the plot at $b=4$ is as shown in Figure 6;

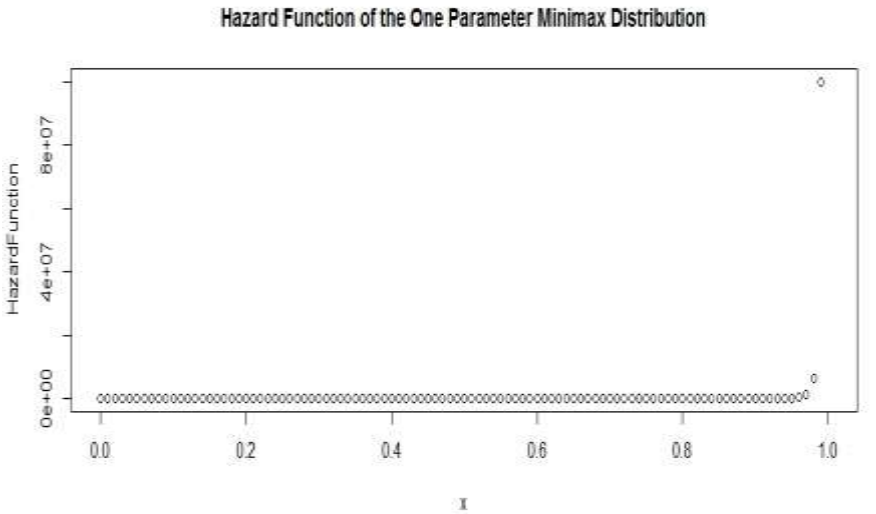

Fig. 6: The Hazard Function of the model when $b = 4$

Figure 6 shows that the proposed model has an increasing hazard rate.

3.0 Estimation

In an attempt to estimate the shape parameter of the proposed model, we employ the use of the method of the Maximum Likelihood Estimation (MLE). Let $X_1, X_2, ..., X_n$ be a random sample of 'n' independently and identically distributed random variables each distributed according to the model defined in Equation (4), the likelihood function L is given by;

$$L(x_1, x_2, ..., x_n \mid b) = \prod_{i=1}^{n} \left[b(1-x)^{b-1} \right]$$

$$= b^n \sum_{i=1}^{n} (1-x_i)^{b-1}$$

Let $l = \log L(x_1, x_2, ..., x_n \mid b)$

$$l = n \ln b + (b-1) \sum_{i=1}^{n} \ln(1-x_i)$$

Differentiating l with respect to 'b' and equating the result to zero gives;

$$\frac{\partial l}{\partial b} = \frac{n}{b} + \sum_{i=1}^{n} \ln(1-x_i)$$

Hence;

$$\sum_{i=1}^{n} \ln(1-x_i) = -\frac{n}{b}$$

$$b = -\frac{n}{\sum_{i=1}^{n} \ln(1-x_i)} \qquad (16)$$

4.0 Conclusion

This article presents a model called One parameter Minimax distribution which was obtained as a special case of both the Beta distribution and the Kumaraswamy distribution. The resulting model is bounded on a (0, 1) support and its shape of the model could be "constant" or "decreasing" (depending on the value of the parameter). Expressions for the rth moment, mean, variance, quantile function, survival function and failure rate are provided. The method

of maximum likelihood estimation (MLE) was proposed in estimating the only parameter in the model. The model shows an increasing hazard rate, thus, we propose the use of the distribution in modeling situations where risk is low at the beginning but increases with time.

References

Johnson, N. L., Kotz, S., and Balakrishnan, N. "Continuous Univariate Distributions", Vol. 2, 2nd Edition, New York: Wiley, 1994

Jones M. C. "The Complementary Beta Distribution", *Journal of Statistical Planning and Inference*, 104, 329-337, 2002

Jones M. C. Kumaraswamy's distribution: "A beta-type distribution with some tractability advantages". *Statistical Methodology*, Vol. 6, 70-81, 2009

Kotz, S., and Van Dorp, J. R. "Beyond Beta; Other Continuous Families of Distributions with Bounded Support and Applications", *World Scientific Press, New Jersey, U.S.A.*, pp: 289, 2004

Kumaraswamy, P. "A generalized probability density function for double-bounded random processes". *Journal of Hydrology*, Vol. 46, 79-88, 1980

Nadarajah, S., and Gupta, A. K. "Generalizations and Related Univariate Distributions," in "Hanbook of Beta Distribution and Its Applications, eds. A.K. Gupta, and S. Nadarajah", *Dekker, New York, U.S.A.*, pp. 97-163, 2004

Oguntunde, P. E., Babatunde, O. S., Ogunmola, A. O. "Theoretical Analysis of the Kumaraswamy-Inverse Exponential Distribution" *International Journal of Statistics and Applications*, Vol. 4, No. 2, 113-116, 2014

Oguntunde, P. E, Odetunmibi O. A, Okagbue H. I, Babatunde O. S, Ugwoke P. O. "The Kumaraswamy-Power Distribution: A Generalization of the Power Distribution" *International Journal of Mathematical Analysis*, Vol. 9, no. 13, 637-645, 2015.

The Impact of Fermentation on the Proximate and Mineral Composition of *Phoenix dactylifera L* Flour

Jokotagba Oloruntobi Adenike[1], Onasanya Seun Sunday[2]
Akinbile Akinlayo Adewale[3]

[1]Department of Science Laboratory Technology
Abaraham Adesanya Polytechnic,
Ijebu- Igbo, Ogun State
E-mail: tobi23_too@yahoo.co.uk
Phone number: +2348034433399

[2]Department of Pharmaceutical Technology
Moshood Abiola Polytechnic,
Abeokuta, Ogun State.

[3]Department of Science Laboratory Technology
Abaraham Adesanya Polytechnic,
Ijebu- Igbo, Ogun State

Abstract: Fermentation was carried out on *Phoenix dactylifera* L. fruit flour. Proximate analysis and mineral analysis were carried out on both fermented and raw sample. The proximate analysis (%) showed that the fermented sample contain higher composition of Moisture, Ash, Crude fat, Crude fibre, and Crude protein except Carbohydrate (64.50 ± 0.01) which is lower compared to the result obtained in the raw sample (76.23 ± 0.02). Mineral analysis (mg/l) of the samples depicted that fermentation increased the Fe (7.64 ± 0.02), Mg (0.96 ± 0.00), Ca (6.26 ± 0.01) and Cu (0.16 ± 0.00) content compared to that of raw Fe (2.17 ± 0.01), Mg (0.94 ± 0.01), Ca (3.13 ±0.07) and Cu (0.13 ± 0.00) in the sample while the composition of Na (1.02 ± 0.90) and K (1.78 ± 0.01) decreased compared with the values of Na (1.28 ± 1.07) and K (2.21 ± 0.02) obtained from the raw fruit flour. The result showed that fermentation transforms the fruit flour into a probiotic food supplement through increased mineral, protein and fibre content thereby enhancing digestibility. The pre-digested carbohydrate content in the fruit flour during fermentation also makes it beneficial for people with diabetes.

Key Words: Fermentation, *Phoenix dactylifera* L, Proximate, Mineral.

Introduction

Fermentation is the process of conversion of sugars to ethyl alcohol under the influence of yeast. Fermentation of sugars by yeast, the oldest synthetic chemical process by man, is still of enormous importance for the preparation of ethanol and certain other alcohols.

Campbell-Platt [1] has defined fermented foods as those foods which have been subjected to the

action of micro-organisms or enzymes so that desirable biochemical changes cause significant modification to the food. However, to the microbiologist, the term "fermentation" describes a form of energy-yielding microbial metabolism in which an organic substrate, usually a carbohydrate, is incompletely oxidised, and an organic carbohydrate acts as the electron acceptor [2]. This definition means that processes involving ethanol production by yeasts or organic acids by lactic acid bacteria are considered as fermentations. Whichever definition used, foods submitted to the influence of lactic acid producing microorganisms is considered a fermented food.

It has been reported that generally, a significant increase in the soluble fraction of a food is observed during fermentation. The quantity as well as quality of the food proteins as expressed by biological value, and often the content of water soluble vitamins is generally increased, while the anti-nutritional factors show a decline during fermentation [3]. Adams [2] also reported that fermentation results in a lower proportion of dry matter in the food and the concentrations of vitamins, minerals and protein appear to increase when measured on a dry weight basis. Meanwhile, according to Khetarpaul and Chauhan [4], single as well as mixed culture fermentation of pearl millet flour with yeast and lactobacilli significantly increased the total amount of soluble sugars, reducing and non-reducing sugar content, with a simultaneous decrease in its starch content.

In addition, Obizoba and Atii [5] stated that combination of cooking and fermentation improved the nutrient quality of sorghum seeds and reduced the content of anti-nutritional factors to a safe level in comparison with other methods of processing while mixed culture fermentation of pearl millet flour with *Saccharomyces diastaticus, Saccharomyces cerevisiae, Lactobacillus brevis* and *Lactobacillus fermentum* was found to improve its biological utilisation in rats [6].

Dates (*Phoenix dactylifera L*) are oval-cylindrical, 3–7 cm long, and 2–3 cm diameter. When ripe, range from bright red to bright yellow in colour, depending on variety. Dates contain a single stone about 2–2.5 cm long and 6–8 mm thick. Three main cultivar groups of date exist: soft, semi-dry and dry and the type of fruit depends on the glucose, fructose and sucrose content [7].

Dates provide a wide range of essential nutrients, and are a very good source of dietary potassium. The sugar content of ripe dates is about 80%; the remainder consists of protein, fiber, and trace elements including boron, cobalt, copper, fluorine, magnesium, manganese, selenium, and zinc [8].

Therefore, the present study aimed at using fermentation process to

produce *Phoenix dactylifera L* flour and carrying out the proximate and mineral composition to enhance its use in different food formulations and recipes.

Materials and Methods

Sample Preparation

Phoenix dactylifera L. fruits were purchased in Ijebu Igbo, Ogun state, Nigeria. The seeds were removed from the fruits after which the mesocarp was sun-dried extensively and ground using a mortal and pestle until a powdery form is obtained. The powdered sample was divided into two portions, half was soaked in a clay pot containing water and left to ferment for 5 days naturally without the introduction of external fermenting micro organisms.

The soaked substrates was then sieved and the fermented sample was sun dried. Both the raw and the fermented samples were kept in an air-tight container and finally placed in a refrigerator prior the analysis.

Proximate Analysis

Proximate analysis (moisture, fat, crude fibre, protein, ash and carbohydrate) of the raw and fermented samples were carried out in triplicate using the methods described by AOAC [9] while the carbohydrate was determined by difference.

Mineral Analysis

The minerals were analysed from solution obtained by first dry-ashing the raw and fermented samples as described by AOAC [10]. Ash was determined by combustion of the sample in a muffle furnace at 550°C for 6 hours. The residue was dissolved in 0.1N HNO_3 to break the ash and the mineral constituents (Ca, K, Mg, Na, Fe, Cu and Pb) were analyzed separately using an atomic absorption spectrophotometer (Analyst 400).

RESULTS

Table 1: Proximate (%) Analysis of Fermented and Raw *Phoenix dactylifera* fruit flour

	Fermented	Raw
Moisture	10.93 ± 0.02	7.32 ± 0.01
Ash	2.71 ± 0.01	2.19 ± 0.01
Crude Fat	14.86 ± 0.00	9.45 ± 0.02
Crude Fibre	4.69 ± 0.02	1.74 ± 0.00
Crude Protein	7.00 ± 0.02	4.81 ± 0.00
Carbohydrate	64.50 ± 0.01	76.23 ± 0.02

Table 2: Mineral (mg/l) Analysis of Fermented and Raw *Phoenix dactylifera* fruit flour

	Fermented	Raw
Iron	7.64 ± 0.02	2.17 ± 0.01
Magnesium	0.96 ± 0.00	0.94 ± 0.01
Calcium	6.26 ± 0.01	3.13 ±0.07
Sodium	1.02 ± 0.90	1.28 ± 1.07
Potassium	1.78 ± 0.01	2.21 ± 0.02
Copper	0.16 ± 0.00	0.13 ± 0.00

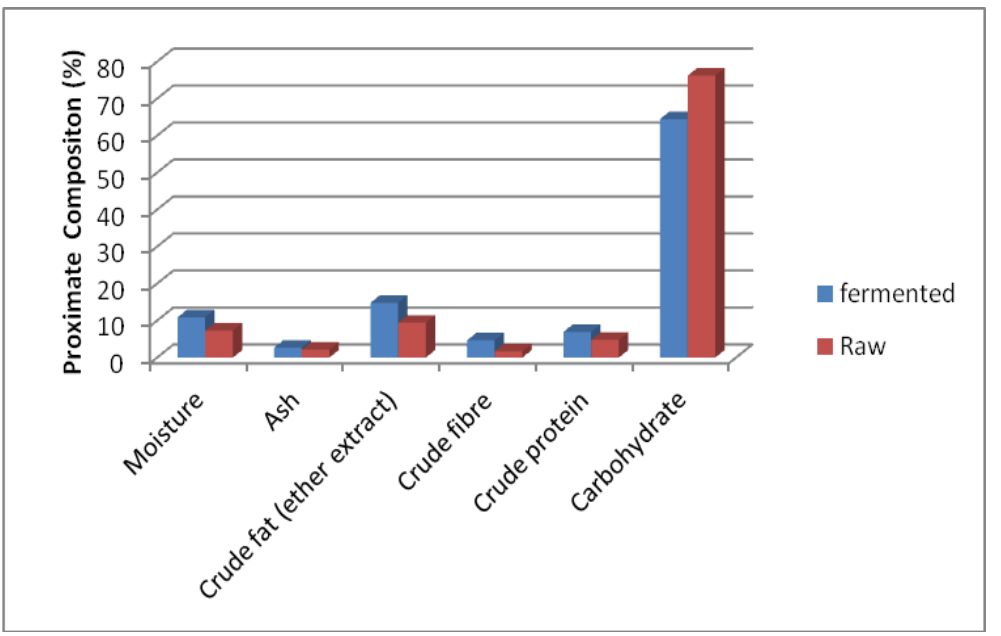

Figure1: Proximate Analysis (%) of Fermented and Raw *Phoenix dactylifera* fruit flour

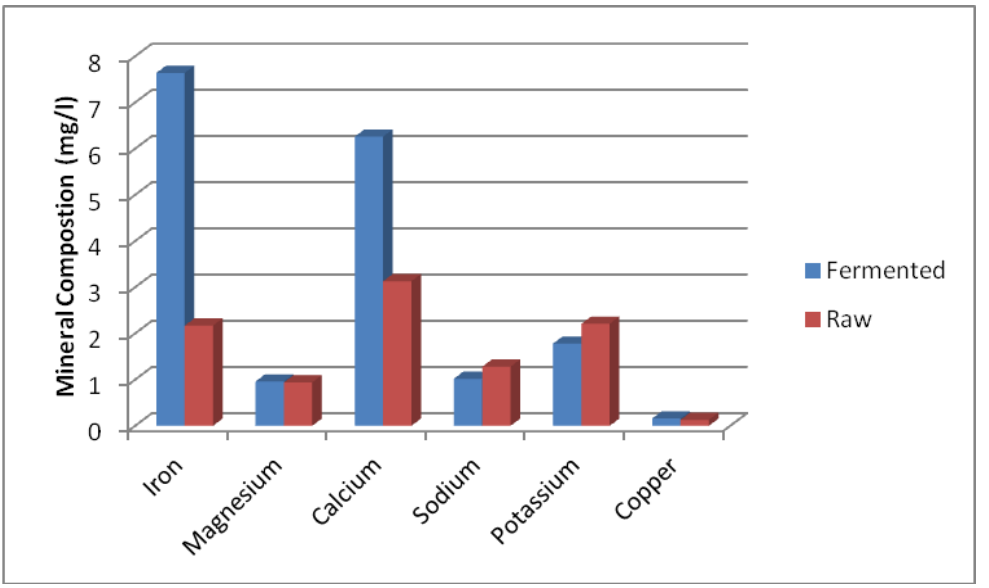

Figure 2: Mineral Analysis (mg/l) of Fermented and Raw *Phoenix dactylifera* fruit flour

Discussion

Result obtained from the proximate analysis of the fermented and raw *Phoenix dactylifera L.* fruit flour as represented in the Table 1 shows that the moisture content of the fermented sample (10.93%) is higher than the value of raw sample (7.32%). This may be due to the absorption of more water through the fermentation process. However, these values are higher than that of Khuzari cultivar (1.6%) reported by Muhammad *et al*. [11].

The decrease in the carbohydrate values because of fermentation may be due to their utilization and transformation by fermentation micro organism to obtain energy and other cellular activities as well as the usual conversion of carbohydrate to ethanol during the process of fermentation. This observation is however similar to that of fermentation by Oladele and Oshodi [12].

However, the crude protein content of the fermented sample is significantly higher compared to the raw samples. Moreover, these values are both higher than that of *Safri cultivar* (2.60%) reported by Kadam *et al.*,[13] but similar to that obtained when pure strain of *Aspergillus niger* was used to ferment maize cobs by Oseni and Ekperigin [14]. This high protein contents could be attributed to the ability of the micro organism to secrete some extra cellular enzymes (proteins) which degrade the materials during fermentation.

The ash content of fermented sample is slightly higher (2.19%-2.71%) than the raw sample, which are both lower than that of Berhi cultivar (2.80%) reported by Kadam *et al.*

[13], this increase may be due to contribution by fermentation micro organisms in the breakdown of the organic components of the fruit samples during the period of fermentation. [12, 14].

The crude fibre content of the fermented sample (4.69%) is higher than that of the raw sample (1.74%) which are both lower than that of Daki cultivar (62.11%) reported by Muhammad *et al.,* [11]. This shows that the fermented fruit can be a good source of dietary fibre which can prevent cardiovascular disease and enhance effective functioning of human digestive tract [15]. In addition, the crude fat (ether extract) of the raw sample is also lower than the value of the fermented sample. These values are both higher than 3.5% reported for millet (*Pennisetum americanum*) [16]. The increase in crude fat could be as a result of extensive breakdown of large molecules of fat into simple fatty acids.

Moreover, the fermentation of *Phoenix dactylifera L.* also caused an increment of most essential mineral contents as presented in Table 2. The content of Fe, Ca, Mg, and Cu present in the fermented sample are higher than that of the raw sample. Meanwhile, values of Na (1.02 ± 0.90) and K (1.78 ± 0.01) of the fermented sample are both lower compared with that of the raw sample whose values are Na (1.28 ± 1.07) and K (2.21 ± 0.02) respectively. This may be due to leaching of soluble minerals into the processing water during the period of the fermentation. In addition, fermenting microorganisms might have used it for metabolic activities as reported by Osman [17].

In conclusion, fermentation increased the protein level; an increase was also discovered in the fat content, crude fibre content and moisture content except for carbohydrate. Fermentation also caused an increase in the availability of some minerals in the sample. Therefore fermented *Phoenix dactylifera L.* fruit can serve as good source of dietary protein, essential minerals for the body and a probiotic food supplement thereby enhancing digestibility.

The decrease in carbohydrate content in the fruit flour during fermentation reduced the sugar content. This makes it beneficial for people with diabetes because fermentation improves pancreatic function, which is of great benefit. Moreso, the carbohydrates in fermented foods have been broken down or pre-digested. As a result, they do not place an extra burden on the pancreas, unlike ordinary carbohydrate.

References

Campbell-Platt G (1987). Fermented foods of the world - a dictionary and guide. London, Butterworths.

Adams M, R (1990): Topical aspects of fermented foods. Trends in

Food Science & Technology 1, pg 141- 144.

Paredes-López O, Harry G, I (1988): Food biotechnology review: traditional solid-state fermentations of plant raw materials - application, nutritional significance and future prospects. CRC Critical Reviews in Food Science and Nutrition 27, pg 159-187.

Khetarpaul N, Chauhan B, M (1990): Fermentation of pearl millet flour with yeasts and lactobacilli: in vitro digestibility and utilisation of fermented flour for weaning mixtures. Plant Foods for Human Nutrition 40, pg 167-173.

Obizoba I, C, Atii J, V (1991): Effect of soaking, sprouting, fermentation and cooking on nutrient composition and some anti-nutritional factors of sorghum (Guinesia) seeds. Plant Foods for Human Nutrition 41, pg 203-212.

Khetarpaul N, Chauhan B, M (1991): Sequential fermentation of pearl millet by yeasts and lactobacilli - effect on the anti-nutrients and in vitro digestibility. Plant Foods for Human Nutrition 41, pg 321-327.

Gepts Paul (2002): The crop of the d ay, "The Date',
http://www.plantsciences.ucdavis.ed u/GEPTS/pb143/CROP/DATE/ date.htm

Bhagwan Das, Sarin, J. L. (1986). "Vinegar from Dates". Industrial & Engineering Chemistry 28 (7): pg 814.

A.O.A.C. (1990): Official Methods of Analysis, Association of Analytical Chemists. 15th ed., Washington D. C. USA. Pg 1121-1180

A.O.AC. (2005): Official Methods of Analysis. 19th Edition. Association of Official Analytical Chemists, Washington, DC. USA. Pg 777-784.

Muhammad Salman Jamil1, Raziya Nadeem, Muhammad Asif Hanif, Muhammad Asif Ali and Kalsoom Akhtar (2008): Proximate composition and mineral profile of eight different unstudied date (*Phoenix dactylifera* L.) varieties from Pakistan, African Journal of Biotechnology Vol. 9(22), pg 3252-3259

Oladele E, P, Oshodi A, A (2008): Effect of fermentation on some chemical and Nutritive properties of Berlandier nettle spurge (*Jatropha cathartica*) and physic Nut (*Jatropha curcas*) seeds. Pakistan Journal of Nutrition, 7, pg 292-296

Kadam P, S, Kale R, V Hashmi S, I (2010): Effect of different varieties of date Palm Paste incorporation on quality characteristics of yoghurt, Research Journal of Diary Science 4 (2), pg 12 -17.

Oseni, O, A, Ekperigin, M. (2007): Studies on biochemical changes in maize wastes fermented with *Aspergillus niger*. Biokemistri, 19: pg 75-79.

Ubom, D, E. (2007): Nutrition, health and our environment. Sendina Ltd, Nigeria. pg 140

Onweluzo J, C, Nwabugwu C, C (2009): Fermentation of Millet (*Pennisetum americanum*) and Pigeon Pea (*Cajanus cajan*) Seeds for Flour Production: Effects on Composition and Selected Functional Properties, Pakistan Journal of Nutrition 8 (6): pg 737-744.

Osman, M, A. (2007): Effect of different processing methods on nutrient composition and anti-nutritional factors and invitro protein digestability of Dolichos lablab beans (Lablab purpureus L) sweet, Pakistan Journal of Nutrition. 6: pg 299-303.

Study on the Potassium content of Nigerian Bananas and the Methanolic Extraction, Phytochemical and Antimicrobial Studies of Oils from Banana Peels

Oluwatosin Y. Audu*, Bamidele M. Durodola*, Raphael C. Mordi*✉, F. Elizabeth Owolabi*, Gabriella C. Uzoamaka*, Joan I. Ayo-Ajayi*, E. Afolake Fadairo*, Ifedolapo O. Olanrewaju*, Taiwo F. Owoeye*, S. John Olurunshola†

*Department of Chemistry and
†Department of Biological Sciences,
School Natural and Applied Sciences,
College of Science and Technology,
Covenant University
Km 10, Idiroko Road,
Ota, Ogun State, Nigeria
raphael.mordi@covenantuniversity.edu.ng

Abstract: Banana is eaten all over the world by all sections of the population. It is known to contain potassium and it has been suggested that it could serve as a source of potassium. Recently, a valuable chemical component, a lectin, called BanLec, was isolated from banana fruit and found to possess anti-HIV-1 activity. However, the peels of banana are thrown away as rubbish and farmers are known to use them as feed for their animals. It is therefore necessary to determine the potassium content of some Nigerian bananas and to also extract the oils from their peels. The components of the extracted oils are to be determined and tested for their biological activity. The potassium content of five (5) varieties of Nigerian bananas (Dwarf Cavendish AAA GP; Lady Finger AA GP; Dwarf Chinese Double; Double Dwarf Senorata AA GP; Giant Cavendish (Williams) AAA GP and Dwarf Red AAA GP) was determined using flame photometer. The potassium content varied from 0.15 mg/g (Dwarf Red) to 1.80 mg/g (Lady Finger). Compared to the value of 358 mg per 100 g reported in the literature, these values are very low and considerable lower than the RDA of 4700 mg. The conclusion is that Nigerian bananas will not be a viable source of potassium for candidates with potassium deficiency. A report on the methanolic extract of oil from their peels is given. Two (2) of the five (5) varieties were chosen and methanolic extraction of oils from their peels was undertaken. The crude extract was subjected to phytochemical analysis, which revealed the presence of the following of steroids, saponin and terpenoids, anthraquinones and tannins. A report is also given on antimicrobial studies of the methanolic extracts, which revealed that the oils were

effective against some bacteria.

Keywords: Banana, Musa acuminata colla, Musa sapientum, methanolic extraction, phytochemical study, microbial study

Introduction

There are different varieties of banana in Nigeria and bananas are excellent sources of potassium, an essential mineral for maintaining normal blood pressure and heart function. It has been suggested that banana could well be a potential source of potassium for people who suffer from potassium deficiency. Potassium or lack of it has been implicated in several physiological and health issues. So it is of interest to determine the amount of potassium in banana to know if by eating banana one could acquire enough potassium required for physiological functions and activities. For example, the importance of potassium ion, K^+, in the Na^+/K^+ pump is well known; its ability to maintain normal fluid and electrolyte balance, as well as facilitating many reactions, supporting cell integrity and in assisting nerve impulse transmission and muscular contraction. Lack of or deficiency in potassium has been implicated in health issues such as muscular weakness, paralysis and confusion as well as potassium's ability to stop the heart if given into the vein; and high blood pressure is associated with low potassium and it has been suggested that high intake of potassium can prevent and correct hypertension [1-3].

An average banana has been reported to contain 467 mg of potassium and only 1 mg of sodium. A banana a day may help to prevent high blood pressure and protect against atherosclerosis. Bananas have long been recognized for their antacid effects that protect against stomach ulcers, heart burns, stress, strokes, pain relief, swelling, itching, bruising, wrinkles, sunburn, gonorrhea and many other ailments. Some of these substances in bananas help activate the cells of the stomach lining, stimulating cell proliferation which thickens the stomach mucosa and act as barrier against stomach acids while others like protease inhibitors help eliminate bacteria in the stomach that are the primary cause of stomach ulcers [4-13]. Animal studies have shown that banana has the potential to lower cholesterol. It was suggested that the dietary fibre component in banana pulp was responsible for its cholesterol-lowering effect. The amount of dietary fibre in banana is relatively constant during banana ripening [14].

They are a good source of carotenoids, which are antioxidants and have a protective effect against chronic disease conditions. Bananas also have a high content of antioxidant phenolic compounds [15-17]. High in iron [18], bananas can

stimulate the production of haemoglobin in the blood and so help in cases of anaemia [19].

Banana peels are rich in fibres and polyphenols, but their composition is dependent on the variety and maturation of the banana [20]. The peels are also rich in carbohydrates and other basic nutrients that can support yeast growth [21-23].

Although banana peels contain low quantities of lignin, they have found use in making charcoal and for the production of value-added products like ethanol, both alternative sources of energy [24, 25].

It is known that banana is a source of potassium and it has been recommended that adult humans consume 4700 milligrams (mg) or more of potassium per day, so it is necessary to determine the potassium content from this source. From the available literature, information is lacking on the potassium content of different varieties of Nigerian banana, so it important to acquire valuable information and to know which variety can provide the most source of potassium. However when banana is consumed the peels are thrown away as waste despite the fact that they are rich in carbohydrate, fibres and polyphenols and their dumping in some cases cause environmental pollution. This agricultural waste is under-utilised, though farmers use it as livestock feed. There is therefore the need to find useful applications for banana peels.

Experiments indicate that if the peels are properly exploited and processed, they could provide high-quality and cheap source of carbohydrates and minerals for livestock [26-28].

The antibacterial and antimicrobial activities, dyeing performance, and effectiveness of banana peels extract have been reported [28-31].

Recently a jacalin-related lectin, BanLec was isolated from banana fruit, Musa acuminata, and was found to inhibit primary and laboratory-adapted HIV-I isolates of different tropisms and subtypes. It possessed potent anti-HIV activity and was found to block HIV-I cellular entry as indicated by temperature-sensitive viral entry studies [32].

With these reports in mind it was decided to investigate efficacy of Nigerian bananas with an initial main objective of identifying and characterizing the chemical constituents of the banana peels.

Materials and Methods

The bananas, Lady Finger AA GP (Musa acuminata colla), Double Dwarf Senorata AA GP (Musa acuminata colla), Dwarf Chinese Double (Musa acuminata colla), Giant Cavendish (Williams) AAA GP (Musa acuminata colla), and Dwarf Red variety AAA GP (Musa acuminata colla) used in this study were obtained from the local market

and their classification confirmed in the Botany Unit of the Biological Sciences department of Covenant University.

For sodium and potassium content, eighty (80) g of each of the five varieties of Nigerian banana (minus the peel) was weighed, crushed with a blender to a homogenous solution with a minimum amount of distilled water. Thereafter 100 cm^3 of 1 mol dm^{-3} HCl (Sigma-Aldrich) was measured and added to each banana solution and placed in an electric shaker set at 200 rpm for 1 h, to ensure homogeneity and complete extraction into solution of potassium and sodium and then centrifuged at 3000 rpm for 30 min for complete separation of the solid particles from the solution. The supernatant layer was collected and stored in polyethylene bottles prior to metal analysis. The clear liquid (0.5 cm^3) was pipetted into a 100 cm^3 standard flask and made up to mark with water. This solution was then analysed for potassium and sodium using flame photometer (Jenway PFP 7). The flame photometer was calibrated with standard solutions of potassium chloride (Sigma-Aldrich).

For oil extraction from the banana peels (two varieties were chosen – Musa acuminata colla (Lady Finger AA GP) and Musa sapientum) about 300 g of the peel was chopped up and put into a thimble for exhaustive Soxhlet extraction using reagent grade methanol as solvent. The methanol was removed on a rotary evaporator to give dark brown oil with chocolate-like smell. Hexane as solvent for extraction was attempted on one banana variety to give clear yellowish oil. The amount of oil obtained from the hexane extraction was very small compared to the amount obtained with methanol as solvent. The oils obtained were stored away from light prior to analysis.

The following microorganisms were used to test the antimicrobial activity of the methanolic extract: *Bacillus spp., Pseudomonas spp., Escherichia coli, Staphylococcus aureus, Streptococcus spp., Klebsiella spp., Proteus spp. and Salmonella spp*. 1 g of the test compound was dissolved in 10 cm^3 of 50% DMSO. The agar well diffusion method was used and the bacteria isolates were standardised with 0.5 M MacFaland standard solution. The isolates were sub-cultured using nutrient agar and incubated for 24 h at 37^{o}C. 0.3 cm^3 of the DMSO solution was then introduced into the bore hole to test for antimicrobial activity. Gentamycin antibiotic was the standard used for analysis. The activity index was computed by subtracting the diameter of the well from the diameter of the clearing zone divided by the diameter of the well.

Results and Discussion

The analysis of the results from the flame photometer indicated the

potassium content as shown in Figure 1.

Figure 1. Potassium content of five (5) varieties of Nigerian bananas (mg/g).

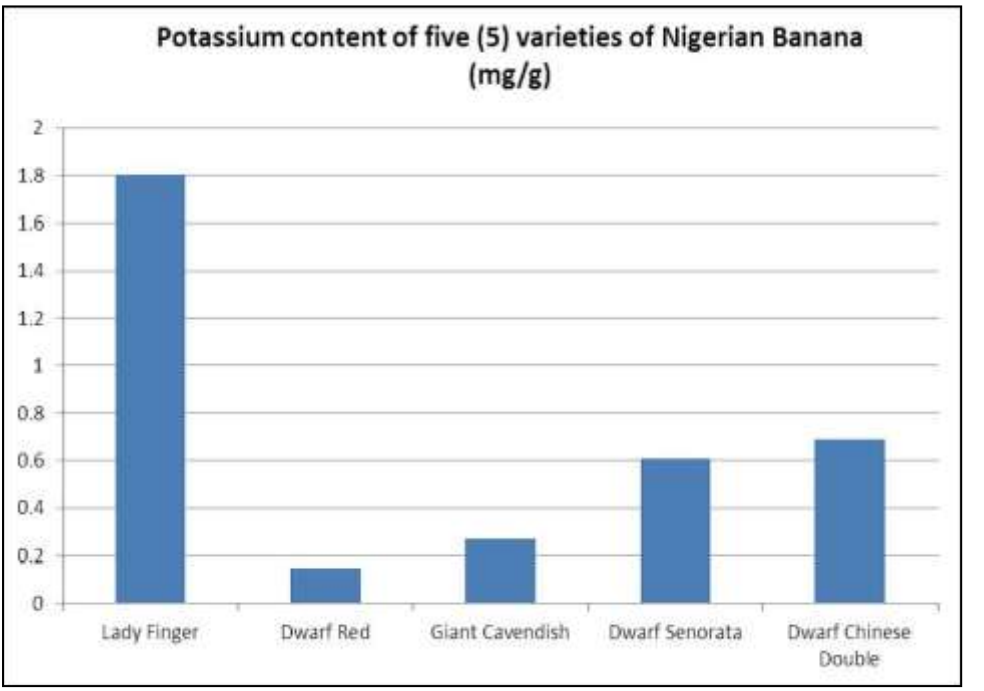

The highest potassium content was found in Lady Finger banana variety. This preliminary finding shows that of the varieties, the Lady Finger variety with 1.80 mg of potassium per gram of banana had 3 times more potassium than the Dwarf Senorata and Dwarf Chinese Double varieties; 6 times more than Giant Cavendish and 12 times more than the Dwarf Red variety. These bananas are grown in different regions of Nigeria, could it then be that the nature of the soil has some influence on the potassium content of the banana?

The potassium content obtained for these varieties of Nigerian banana, when compared to an average value of 3.58 mg of potassium in 1 g of a different variety of banana [33], are significantly smaller. Lady Finger, the banana with the highest potassium content (1.8 mg/g) has about half this average value.

Qualitative phytochemical screening of the methanolic extract of the two bananas shows (Table 1) the presence of saponin, anthraquinones, terpenoids, steroids, tannins and trace amounts of phenols. Some of these compounds have been reported to be present in peel extracts [34].

Table 1. Phytochemical screening for crude methanolic extract (+ = present and – = absent)

	Musa acuminata colla	***Musa sapientum***
Saponin	–	–
Anthraquinones	–	++
Terpenoids	++	++
Tannins	++	++
Steroids	++	++
Phenols	Trace	Trace
Flavonoids	–	–

Table 2. Antimicrobial test results on the crude methanolic extract (R = not responsive)

Organism	**Clearing zone (mm)**			**Activity Index**	
	Sample (0.3 cm^3)				
	Musa acuminata colla	***Musa sapientum***	**Gentamycin Standard**	***Musa cuminata colla***	***Musa sapientum***
Bacillus spp.	9.00	7.00	26.00	0.65	0.73
Staphylococcus aureus	12.00	7.00	25.00	0.52	0.72
Pseudomonas spp.	10.00	6.00	26.00	0.62	0.77
Escherichia coli	11.00	7.00	22.00	0.50	0.68
Streptococcus spp.	16.00	10.00	22.00	0.27	0.55
Klebsiella spp.	10.00	12.00	22.00	0.55	0.45
Proteus spp.	5.00	R	25.00	0.80	–
Salmonella spp.	R	R	R	–	–

Preliminary results of the antimicrobial tests (Table 2.) showed that the extract was active against the test organisms used except *Salmonella spp. Proteus spp.* was also not responsive to Musa sapientum. The activity index for these extracts shown in the table it can be seen that they are effective against the bacteria shown, however not as effective as the Gentamycin standard. It is however thought that

increasing the concentration of these extracts their effectiveness might be as high as that of Gentamycin standard.

Conclusion

The preliminary results from these experiments suggest that these bananas would not be significant sources of potassium since the highest potassium content is 1.80 mg in 1 g of banana from Lady Finger banana (Musa acuminata colla). The methanolic extracts were found to have antimicrobial activity against the test organisms used and we are making effort to identify the constituents of the extracts in order to identify the components that may be responsible for the antimicrobial activity.

References

Devlin, T. M. (2006) Editor Textbook of Biochemistry with Clinical Correlations, 6th ed., Wiley-Liss, page 986

Berg, J. M., Tymoczko, J. L. and Stryer, L. (2007) Biochemistry, 6th ed., W. H. Freeman and Co., page 354

Whitney, E. and Rolfes, S. R. (2005) Understanding Nutrition (ISE), 10th ed., Thomson-Wadsworth, page 411

Wath, J. N. and Brayer-Brand Wijk, M. G. (1962) The medicinal and poisonous plants of south and eastern Africa, 2nd ed., E. & S. Livingstone Ltd, Edinburgh and London.

Edwards, B. (1999) Banana peels extract composition and method of extraction – Patent No WO 99/38479.

Quisumbing, E. (1978) Medicinal plants of the Philippines, Manila: Bureau of Printing, pp 553 – 554.

Ghani, A. (2033) Medicinal plants of Bangladesh: Chemical constituents and uses – 2nd ed. Dhaka, The Asiatic Society of Bangladesh, pp 315, 500 – 505.

Khare, B. P. Ed., (2007) Indian Medicinal plants, Springer Science and Business Media, New York, USA, p 426.

Partha, P and Hossain, A. B. M. E. (2007) Ethnobotanical investigation into the Mandi Ethnic community in Bangladesh, Bangladesh J. Plant Taxon., **14**, 129 – 145.

Goel, R. K. and Sairam, K. (2002) Anti-ulcer drugs from indigenous sources with emphasis on *Musa sapientum*, *Tamrabhasma*, *Asparagus racemosus* and *zingiber officinale*, Indian J. Pharmacol., **34**, 100 – 110.

Agarwal, P. K., Singh, A., Gaurav, K., Goel, S., Khana, H. D. and Goel, R. K. (2009) Evaluation of wound healing activity of extracts of plantain banana (*Musa sapientum var. paradisiaea*) in rats, Indian J. Exp. Biol., **47**, 322 – 340.

Tewtrakul, S., Itharat, A., Thammaratwasik, P. and Ooraikul, P. (2008) Anti-allergic and antimicrobial activities of some Thai crops – Songklanakarin J Sci. Technol., **30**(4), 467 – 473.

Jain, D. L., Baheti, A. M., Parakh, S. R., Ingale, S. P. and Ingale, P. L. (2007) Study of antacid and diuretic activity of ash and

extracts of *Musa sapientum* L. fruit peel, Phcog Mag., **3**, 116 – 119.

Sampath Kumar, K. P., Bhowmik, D., Duraivel, S. and Umadevi, M. (2012) Traditional and medicinal uses of banana, J. Pharmaocgn. Phytochem., **1**, 57 – 70.

Nagarajaiah, S. B. and Prakash, J. (2011) Chemical composition and antioxidant potential of peels from three varieties of banana, Asian J. Food and Agro-Industry, **4**, 31 – 36.

Baskar, R., Shrisakthi, S., Sathyapriya, B., Shyampriya, R., Nithya, R. and Poongodi, P. (20011) Antioxidant potential of peel extracts of banana varieties (*Musa sapientum*), Food Nutri. Sci., **2**, 1128 – 1133.

Darsini, D. T. P., Maheshu, V., Vishnupriya, M. and Sasikumar, J. M. (2012) In vitro antioxidant activity of banana (*Musa ssp. ABB cv. Pisang Awak*), Indian J. Biochem. Biophys., **49**, 124 – 129.

Aremu, C. Y. and Udoessien, E. I. (1990) Chemical estimation of some inorganic elements in selected tropical fruits and vegetables, Food Chem., **37**, 229 – 240.

Akinyosoye, V. O. (1991) Tropical Agriculture, Macmillian Publishers, Ibadan, pp 65 – 68.

Happi Emaga, T., Andrianairo, R. H., Wathelet, B., Tchango, J. T. and Paquot, M. (2007) Effect of the stage of maturation and varieties on the chemical composition of banana and plantain peels Food Chem., **103**, 590 – 600.

Brooks, A. (2008) Ethanol production potential of local yeast strains isolated from ripe banana peels, African J. Biotech., **7**, 3749 – 3752.

Essien, J. P., Akpan, E. J. and Essien, E. P. (2005) Studies on mould growth and biomass production using waste banana peels, Bio-resource Technology, **19**, 361 – 363.

Hueth, B. and Melkonyan, T. (2004) Quality Measurement and contract design, Lessons from the North American Sugar beet Industry, Canadian J. Agric. Econ., **52**, 165 – 181.

Singh, A. K., Rath, S., Kumar, Y., Masih, H., Peter, J. K., Benjamin, J. C., Singh, P. K. and Singh, D. P. (2014) Bio-ethanol production from banana peel by simultaneous saccharification and fermentation process using co-cultures *Aspergillus niger* and *saccharomyces cerevisiae,* International J. Current Microbiology and Applied Sciences, **3**, 84 – 96.

Kudan, M. J. (1962) Encyclopedia of fruits, vegetables, nuts and seeds for healthful living, Parker Publishers Inc. Hattiesburg, Maryland.

Anhwange, B. A., Ugye, T. J. and Nyiaatagher, T. D. (2009) Chemical composition of Musa sapientum (banana) peels, Electronic J. Environ. Agric. Food Chem., **8**, 437 – 442.

Chandraju, S., Mythily, R. and Chidan, K. C. S. (2011) Extraction, isolation and identification of sugars from banana peels (Musa

sapientum) by HPLC coupled LC/MS instrument and TLC analysis, J. Chem. Pharm. Res., **3**, 312 – 321.

Shah, A. M., Qureshi, M., Memo, Z. N., Memon, S. N. and Syed, S. K. (2012) Analysis of carbohydrate and protein from pulp and peel of apple (*Malus sylvestis*) and banana (*Musa paradisiacal*), Sindh Univ. Res. J. (Sci. Ser.), **44**, 71-74.

Salah, S. M. (2013) Antibacterial activity and ultraviolet (UV) protection property of some Egyptian cotton fabrics treated with aqueous extract from banana peel, African J. Agric. Res., **8**, 3994 – 4000.

Fagbemi, J. F., Ugoji, E., Aderipekun, T. and Adelowoton, O. (2009) Evaluation of the antimicrobial properties of unripe banana (*Musa sapientum* L.), lemon grass (*cymbopogon citratus* S.) and turmeric (*Curcuma longa* L.) on pathogens, African J. Biotechnol., **8**, 1176 – 1182.

Rogasa, C. Y., Martinez, A. T., Chua, J. E. Y. and Rideout,J. A. (2007) A Triterpene from *Musa errans*, Philippine J. Sci. **136**, 167 – 171.

Swanson, M. D., Winter, H. C., Goldstein, I. J. and Markovitz, D. M. (2010) A Lectin isolated from banana is a potent inhibitor of HIV replication, J. Biol. Chem., **285**(12), 8646 – 8655.

USDA Nutrient Database for Standard Reference (http://www.nal.usda.gov/fnic/foodcomp/search/)

Zafar, M., Saleha, A., Ehsanul Hoque, M. Md. and Sohel, R. Md. (2011) Antimicrobial and cytotoxic properties of different extracts of *Musa sapientum L. subsp. Sylvestris*, International Res. J. Pharm. **2**, 62 – 65.

The involvement of free radicals in the mechanism of β-Carotene Degradation

Raphael C. Mordi

Chemistry Department,
College of Science and Technology,
Covenant University,
Km 10, Idiroko Road, Ota, Ogun State.
raphael.mordi@covenantuniversity.edu.ng

***Abstract*:** β-Carotene, a pro-vitamin A carotenoid, was reacted with oxygen in benzene as solvent, in the dark. The products of oxidation were characterised by HPLC with a UV photodiode detector and LC-MS, EI mode. The products identified were oxygen-containing compounds of the type epoxides, aldehydes and ketones. ESR study of retinyl- and ionyl-derivatives revealed that the secondary sites C7 and C9 were the most reactive towards radical generation. Both the results of product analysis and the ESR study enabled us to propose that the products of β-carotene autoxidation were obtained by a free radical mechanism involving initial formation of a biradical during the *trans*-to-*cis* isomerisation at the 15,15' bond and attack by oxygen.

***Keywords*:** Carotene, Carotenoids, Apo-carotenoids, ESR, Degradation, Autoxidation, Free radicals.

Introduction

β-Carotene is a pro-vitamin A carotenoid possessing half the activity of vitamin A. Because of its structural resemblance to vitamin A, it was thought that two molecules of vitamin A could be obtained by central cleavage from β-carotene (Karrer et al. [1]). However, attempts to obtain two molecules of vitamin A directly from β-carotene have, so far, failed. In the absence of antioxidants, the carotenoids are unstable to heat, light and air/oxygen. Peto et al., [2] suggested that dietary β-carotene might function as an anti-carcinogenic agent. In both in vitro and in vivo studies β-carotene has been shown to act as both a pro-oxidant and an antioxidant, Packer et al. [3]; Krinsky and Deneke [4].

The question that has often arisen is whether it is β-carotene per se or its degradation products that is responsible for its antioxidant activity? In addition, the mode of action whereby β-carotene is degraded is largely unknown. It is the elucidation of this latter unknown aspect that is the objective of this paper through an examination of the products of β-carotene oxidation and an ESR study of reactive intermediates from retinyl- and

ionyl-derivatives. We propose the evidence as strongly favouring the involvement of free radicals in the degradation of β-carotene.

Materials and Method

β-Carotene, β-ionone, β-cyclocitral, retinyl acetate, *cis*-9-retinal, *cis*-13-retinal and β-apo-8'-carotenal were obtained from Sigma-Aldrich. The epoxy compounds were prepared as described by Barber et al. [5], and the other relevant compounds were prepared according to the literature methods described in Haag et al. [6], Attenburrow et al. [7], Huisman et al. [8] and Haeck et al. [9]. The details of the experimental method for β-carotene oxidation can be found in Mordi et al. [10].

Results and Discussion

The products of β-carotene autoxidation identified by following the progress of reaction are listed in Figure 1. This list has been compiled from these references Mordi et al. [10]; Tang et al. [11]; Wang et al. [12], and Rodriguez and Rodriguez-Amaya [13].

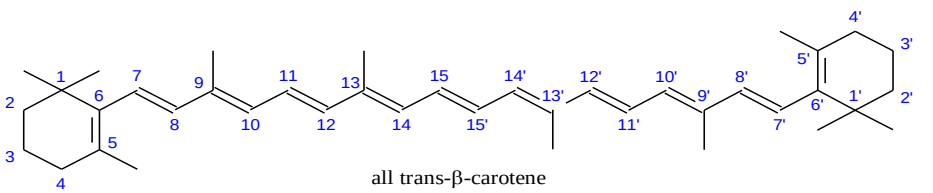

all trans-β-carotene

Product name	Structure
15,15'-epoxy-β-carotene	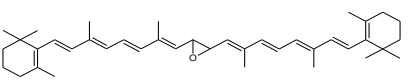
5,6-epoxy-β-carotene	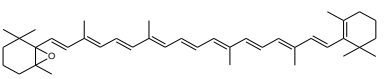
5,6,5',6'-diepoxy-β-carotene	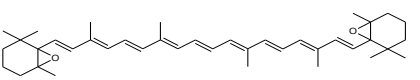
5,8-epoxy-β-carotene	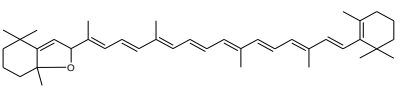
5,8,5'8'-diepoxy-β-carotene	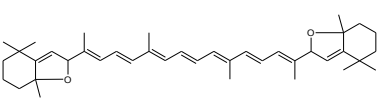
β-apo-12'-carotenal	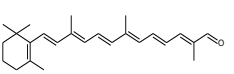
β-apo-14'-carotenal	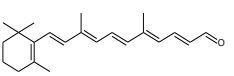

Retinal 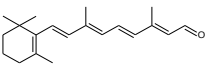

β-apo-13-carotenone 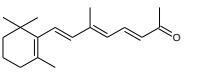

β-ionylidene acetaldehyde 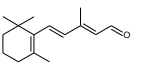

β-ionone 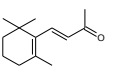

β-apo-10'-carotenal 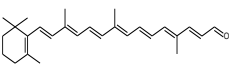

5,6-epoxy-β-ionone 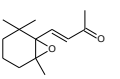

β-cyclocitral 

Dihydroactinidiolide 

4-oxo-β-ionone 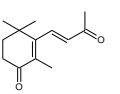

2,2,6-trimethylcyclohexanone 

Fig 1 Products of β-Carotene oxidation

It is suggested that free radicals are involved in the oxidation, since the extended system of conjugated double bonds makes β-carotene susceptible to radical attack. Evidence for the involvement of free radicals in the oxidation of β-carotene is that the oxidation is accelerated by radical initiators (AIBN) and inhibited by radical chain-breaking antioxidants BHT and α-tocopherol. So how do these products arise? Zechmeister et al. [14] and El-Tinay and Chichester [15], suggested that the central double bond of β-carotene is less susceptible to oxidative attack than the terminal double bonds, which are the sites of greatest electron density. Glover [16], suggested that the degradation of β-carotene proceeded by initial attack at one end of the molecule, forming a series of apo-carotenoids by the removal of two carbon units. The initial evidence for these carotenoids was presented by Sharma et al. [17]. Mohamed et al. [18] and Doering and Sarma [19] recently confirmed that the terminal double bonds were the preferred sites of attack as there is a greater loss of stabilisation energy the radical formed as we move away from the centre of the polyene chain

compared to the loss towards the centre.

In our ESR study of retinyl- and ionyl-derivatives and spin trapping of the radicals generated from them, we were able to show that C7 and C9 for ionyl-derivatives and C7, C9 and C11 and probably C15 for retinyl-derivatives were the most reactive sites, Mordi and Walton [20]. Apart from C15, which is a primary site, these sites are secondary. The radical generated will, of course, be delocalised over several carbon atoms and the terminal carbons will be the most sterically exposed and so more susceptible to attack. By extension therefore, it is suggested that these sites would be vulnerable to attack on the conjugated system of β-carotene.

A study of self-initiated autoxidation of retinal showed that retinal is resistant to oxidation compared to β-carotene, Mordi et al. [10]. ESR study of retinal failed to give any ESR signal. Retinyl derivatives gave only a broad and weak ESR spectrum, Mordi and Walton [20]. Could this be an indication that there is a predetermined chain length to allow for isomerisation before biradical formation?

The lack of reactivity of retinol could be attributed to the compound's inability to undergo the initial *cis-trans* isomerisation at the C15 carbon atom and the presence of the hydroxyl group preventing the initial epoxide formation at C15. The observed products after prolonged reaction time could be due to end-chain peroxyl attack on retinal. Although retinal is known to undergo *cis-trans* isomerisation at C11 for vision, if this happened in the oxidation reaction system, through the suggested biradical mode, the biradical would not be as strongly stabilised (delocalised) as the biradical derived from β-carotene and therefore more energy would be needed to bring about its formation.

It is thought that the mechanism of autoxidation begins by an initial *trans-cis* isomerisation at 15,15' central double bond, Mordi et al. [10] and Doering and Sarma [19]. The original idea of the involvement of *cis* isomer was put forward by Glover [16] and recent studies have shown that *cis* isomers are truly involved in β-carotene autoxidation and degradation. We showed that there were other isomers of β-carotene in the product mixture during oxidation but were unable to properly identify which isomers. Other workers have been able to identify these isomers as 9-cis and 13-cis-β-carotene, Mohamed et al. [18], Penicaud et al. [21], Achir et al. [22], Marx et al. [23] and Henry et al. [24]. This trans-cis isomerisation implies the formation of a biradical intermediate, Mordi et al. [10].

The likelihood of involvement of free radicals is enhanced by the fact that the products of β-carotene oxidation by molecular oxygen are similar to those obtained by singlet oxygen oxidation. The similarity of products in these reactions has led to the suggestion that a singlet biradical

of β-carotene is formed in the *cis* configuration, which is stabilised by extensive delocalisation of the two unpaired electrons. The biradical is then attacked by oxygen on either side of the *cis* bond leading to the formation of carotenyl peroxyl triplet biradical, Scheme 1 and Scheme 2.

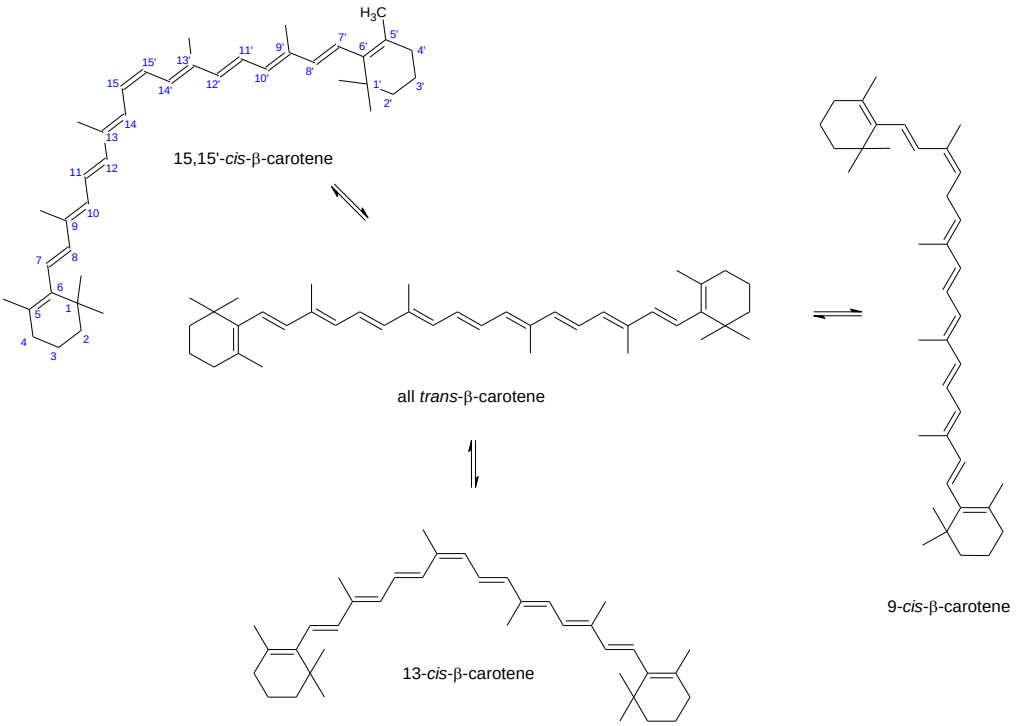

Scheme 1. Cis-trans isomerisation of all-trans-β-carotene prior to formation of the biradical, (Mordi et al. [10]; Mordi [25], and Penicaud et al. [21].)

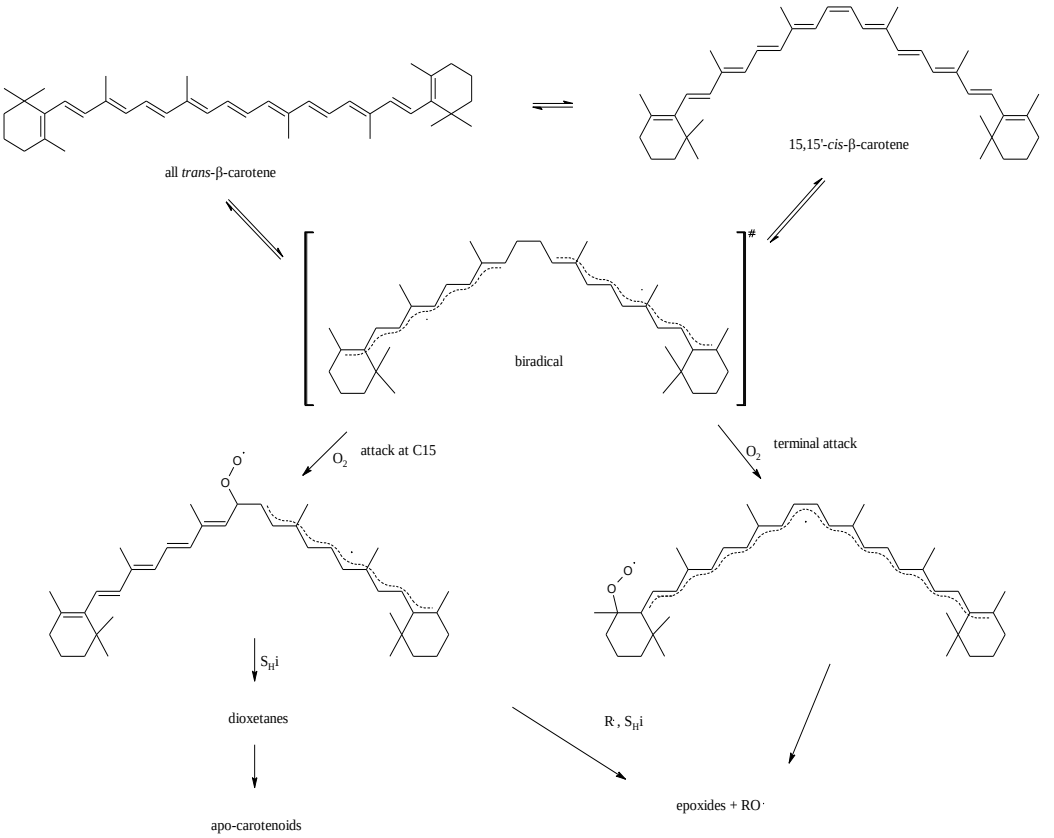

Scheme 2. Steps in the formation of oxidation products, (Mordi et al. [10], Mordi [25] and Penicaud et al. [21].)

These peroxyl triplet radicals are sufficiently long-lived to act as initiators of autoxidation.

Following homolytic intramolecular substitution, S_Hi, (Mayo [26]; Mayo and Miller [27]; Porter et al. [28], and Porter and Zuraw, [29]), the peroxyl biradicals will collapse most probably by hydrogen abstraction to give hydroperoxides, thereby allowing the epoxides to appear as products whereas attack by oxygen at any position of the biradical would give the apo-carotenoids. By monitoring the progress of reaction, it was shown that the apo-carotenoids begin to appear at the same time, Mordi et al. [10].

By following the progress of reaction we have shown that all the double bond positions are vulnerable to attack by oxygen, but the initial site of attack appears to be at the terminal and central double bonds, as 5,6-epoxy, 5,6,5',6'-diepoxy and 15,15'-epoxy carotenes were identified at the initial stages of reaction. The attack at 15,15' double bond would probably lead to formation of dioxetane, which eventually collapses to the apo-carotenoids detected, whereas attack

at the terminal double bonds would lead to the epoxides. The apo-carotenoids were also identified, again suggesting the vulnerability of all the double bond positions (Mordi, [25]). These cleavage products have been identified by other workers and the formation of in-chain epoxides has been suggested as precursors to apo-carotenoids (Rodriguez and Rodriguez-Amaya [13]; Hiranvarachat et al. [30]; Caris-Veyrat et al. [31]). The formation of 5,8-epoxy- and 5,8,5',8'-diepoxy-β-carotene has been linked to the acid catalysed isomerisation of the 5,6-epoxy equivalents in food ripening (Rodriguez and Rodrigues-Amaya [13]) . We also suggested that these furanoids are formed directly from the peroxyl radicals.

Conclusion

We can conclude that β-carotene is degraded by initial *cis-trans* isomerisation, followed by the formation of a singlet biradical. The biradical is then attacked by oxygen to produce peroxyl radicals at the double bonds. The peroxyl radicals at the terminal double bonds are transformed to epoxides and furanoids and along the chain are transformed to apo-carotenoids.

Acknowledgements: I am deeply grateful to Professor John Walton, University of St. Andrews, Scotland for the opportunity he gave me, his continued support and encouragement. I also gratefully acknowledge the support of Agriculture and Food Research Council; Royal Society; Association of International Cancer Research; National Foundation for Cancer Research, and NATO.

References

Karrer, P., Morf, R. and Schopp, K. (1931) Zur kenntnis des vitamins-A aus fischtranen II, Helv Chim Acta, **14**, 1431 – 1436

Peto, R., Doll, R., Buckley, J. D. and Sporn, M. B. (1981) Can dietary beta carotene materially reduce human cancer rates? Nature, **290**, 201 – 208

Packer, J. E., Mahood, J. S., Mora-Arellano, V. O., Slater, T. F., Wilson, R. L. and Wolfenden, B. S. (1981) Free radicals and singlet oxygen scavengers: Reaction of a peroxyl-radical with β-carotene, diphenyl furan and 1,4-diazobicyclo(2,2,2)-octane, Biochem Biophys Res. Commun, **98**, 901 – 906

Krinsky, N. I. and Deneke, S. M. (1982) Interaction of oxygen and oxy-radicals with carotenoids, J Natl Cancer Inst, **69**, 205 – 210

Barber, M. S., Davies, J. B., Jackman, L. M. and Weedon, B. C. L. (1960) Studies in nuclear magnetic resonance. Part I. Methyl groups of carotenoids

and related compounds, J Chem Soc, 2870 – 2881

Haag, A., Eschenmoser, W. and Eugster, C. H. (1980) Synthesis von (-)-(*R*)-4-Hydroxy-□-ionon und (-)-(*5R,6S*)-5-Hydroxy-4,5-dihydroxy-β-ionon aus (-)-(*S*)-β-ionon, Helv Chim Acta, **63**, 10 – 15

Attenburrow, J., Cameron, A. F. P., Chapman, J. H., Evans, R. M., Hems, B. A., Jansen, A. B. A. and Walker, T. W. (1952) A synthesis of vitamin A from cyclohexanone, J Chem Soc, 1094 – 1111

Huisman, H. O., Smit, A., van Leewan, P. H. and van Rij, J. H. (1956) Investigations in the vitamin A series. III. Rearrangement of the retro-system to the normal system of conjugated double bonds in the vitamin A series, Recl Trav Chim Pays-Bas, **75**, 977 – 1006

Haeck, H. H, Kralt, T. and van Leewan, P. H. (1966) Synthesis of carotenoidal compounds. I. Preparation of some substituted Polynesia with cross-conjugation, Recl Trav Chim Pays-Bas, **85**, 334 – 338

Mordi, R. C., Walton, J. C., Burton, G. W., Hughes, L., Ingold, K. U., Lindsay, D. A. and Moffatt, D. J. (1993) Oxidative Degradation of β-Carotene and β-Apo-8'-Carotenal, Tetrahedron, **49** (4), 911 – 928

Tang, G., Wang, X-D., Russell, R. M. and Krinsky, N. I. (1991) Characterisation of β-Apo-13-carotenone and β-Apo-14'-carotenal as enzymatic products of the excentric cleavage of □-carotene, Biochemistry, 30, 9829 – 9834

Wang, X-D., Tang, G., Fox, J. G., Krinsky, N. I. and Russell, R. M. (1991) Enzymatic conversion of β-carotene into β-apo-carotenals and retinoids by human, monkey, ferret and rat tissues, Arch Biochem Biophys, 285, 8 – 16

Rodriguez, E. B. and Rodriguez-Amaya, D. B. (2007) Formation of apo carotenals and epoxy carotenoids from β-carotene by chemical reactions and by autoxidation in model systems and processed foods, Food Chem, **101**, 563 – 572

Zechmeister, L., Le Rosen, A. L., Schoeder, W. A., Polhar, A. and Pauling, L. (1943) Spectral characteristics and configuration of some stereoisomeric carotenoids including prolycopene and pro-β-carotene, J Am Chem Soc, **65**, 1940 – 1951

El-Tinay, A. H. and Chichester, C. O. (1970) Oxidation of β-carotene. Site of initial attack, J Org Chem, **35**, 2290 – 2293

Glover, J. (1960) The conversion of β-carotene to vitamin A, Vitam Horm, **18**, 371 – 386

Sharma, R. V, Mathura, S. N., Dmitrovskii, A. A., Das, R. S. and Ganguly, J. (1976) Studies on the metabolism of β-carotene and apo-β-carotenoids in rats

and chickens, Biochem Biophys Acta, **486**, 183 – 94

Mohamed, N., Hashim, R., Rahman, N. A. and Zain, S. M. (2001) An insight into the cleavage of β-carotene to vitamin A: a molecular mechanics study, J Mol Struct, **538**, 245 – 252

Doering, W. von E. and Sarma, K. (1992) Stabilisation energy of polyethylene radicals: all *trans*-nonatetraenyl radical by thermal rearrangement of a semirigid {4-1-2}heptane. Model of thermal stability of β-carotene, J Am Chem Soc, **114**, 6037 – 6043

Mordi, R. C. and Walton, J. C. (1990) Electron spin resonance study of free radicals generated from retinyl- and ionyl-derivatives, Chem Phys Lipids, **54**, 73 – 78

Penicaud, C., Achir, N., Dhuique-Mayer, C., Dornier, M. and Bohuon, P. (2011) Degradation of β-carotene during fruit and vegetable processing or storage: reaction mechanisms and kinetic aspects: a review, Fruits, **66** (6), 417 – 440

Achir, N., Penicaud, C., Avallone, S. and Bohuon, P. (2011) Insight into β-carotene thermal degradation in oils with multipurpose modelling, J Am Oil Chem Soc, **88** (12), 2035 – 2045

Marx, M., Stuparic, M., Schieber, A. and Carle, R. (2003) Effect of thermal processing on *trans*-*cis*-isomerisation of β-carotene in carrot juices and carotene-containing preparations, Food Chem, **83**, 609 – 617

Henry, L. K., Catignani, G. and Schwartz, S. (1998) Oxidative degradation kinetics of lycopene, lutein and 9-*cis* and all-*trans*-β-carotene, J Am Oil Chem, Soc., **75**, 823 – 829

Mordi, R. C. (1993) Carotenoids: Functions and Degradation, Chem Ind, 79 – 83

Mayo, F. R. (1958) The oxidation of unsaturated compounds V. The effect of oxygen pressure on the oxidation of styrene, J Am Chem Soc, **80**, 2465 – 2480

Mayo, F. R. and Miller, A. A. (1958) The oxidation of unsaturated compounds VI. The effect of oxygen pressure on the oxidation of β-methylstyrene, J Am Chem Soc, **80**, 2480 – 2493

Porter, N. A., Cudd, M. A., Miller, R. W. and McPhail, A. T. (1980) A fixed geometry study of the S_H2 reaction on the peroxide bond, J Am Chem Soc, **102**, 414 – 416

Porter, N. A. and Zuraw, P. J. (1984) Stereochemistry of hydroperoxide cyclisation reactions, J Org Chem, **49**, 1345 – 1348

Hiranvarachat, B., Suvarnakuta, P. and Devahastin, S. (2008) Isomerisation kinetics and autoxidant activities of β-carotene in carrots undergoing different drying techniques and conditions, Food Chem, **107**, 1538 – 1546

Caris-Veyrat, C., Arniot, M. J., Ramasseul, R. and Marchon, J. C. (2001) Mild oxidative cleavage of β-carotene by dioxygen induced by a ruthenium porphyrin catalyst: characterisation of products and some possible intermediates, New J Chem, **25**, 203 – 206

Kinetics, Isotherms and Thermodynamics Studies of Sorption of Cu^{2+} onto Novel Zerovalent Iron Nanoparticles

A.O. Dada[1*], F.A. Adekola[2] and E.O. Odebunmi[3]

[1*]Department of Physical Sciences (Industrial Chemistry Programme), Landmark University, P.M.B.1001, Omu-Aran, Kwara State, Nigeria.
[2]Department of Industrial Chemistry, University of Ilorin, P.M.B. 1515, Ilorin, Nigeria.
[3]Department of Chemistry, University of Ilorin, P.M.B. 1515, Ilorin, Nigeria.

**Corresponding author*: dada.oluwasogo@lmu.edu.ng

***Abstract*:** A novel nanoscale zerovalent iron (nZVI) is an effective adsorbent for scavenging inorganic and organic toxicants. nZVI was synthesized in a single pot system using bottom-up approach and were characterized by BET, SEM, EDX and FTIR. In this study, sorption of Cu^{2+} onto nZVI was carried out vis-à-vis the investigation of physicochemical parameters (initial metal ion concentration, pH, temperature, adsorbent dose) at 298 K. The sorption data obtained at optimum conditions were subjected to six different isotherm models (Langmuir, Freundlich, Temkin, Dubinin-Raduskevich (D-R), Halsey and Harkin-Jura). However, the equilibrium sorption data were best described by both Langmuir and Temkin isotherm models with Langmuir maximum monolayer coverage (Q_{max}) of 40.816 mg/g and regression correlation value ($R^2 > 0.96$) supporting a chemisorption mechanism. Pseudo first-and second-order, Elovich, fractional power and intra-particle diffusion models were applied to the adsorption data in order to investigate the kinetic process; pseudo second-order fitted the data most. The intra-particle diffusion model suggested that the intra-particle diffusion was one of the rate-limiting steps. The values of the Gibbs free energy showed the feasibility and spontaneity of the sorption process. The removal efficiency of Cu^{2+} (> 98%) onto zerovalent iron nanoparticles revealed that nZVI is a promising and efficient adsorbent that can be utilized by industries on a large scale for waste treatment.

Keywords: Zerovalent Iron nanoparticle; Sorption; Isotherms; Kinetics and Thermodynamic

Introduction

Copper is a transition metal and one of the heavy metals in group 1B with density of 8.9 $g.cm^{-3}$. It is released into the environment through natural phenomena and anthropogenic activities and these account for its wide spread in the environment. Copper is often found near mines, industrial settings, landfills and waste disposals. Most copper compounds will settle and be bound to either water sediment or soil particles. Soluble copper compounds form the largest threat to human health. Usually, water-soluble copper

compounds occur in the environment after release through application in agriculture. Copper in the blood exists in two forms either bound to *ceruloplasmin* or the rest "free", loosely bound to albumin and small molecules. Free copper causes toxicity, as it generates reactive oxygen species such as superoxide, hydrogen peroxide and the hydroxyl radicals all of which damage proteins, lipids and DNA [1]. There are a number of adverse effects of copper due to over-exposure such as: irritation of the nose, mouth and eyes, headaches, stomachaches, dizziness, vomiting, *hematemesis*, diarrhea, hypotension, melena, coma, jaundice. Intentionally, high uptakes of copper may cause liver and kidney damage and even death [2].

Nanoparticles are the new trend of effective adsorbents used in the decontamination of water and immobilization of heavy metal ions from their solutions. Research on the utilization of nanoparticles is on the increase due to their special characteristics. Various methods have been reported by researchers for the removal of heavy metal ions from the environments such as chemical precipitation [3], ion exchange [4], solvent extraction [5], ultra-filtration [6], reverse osmosis [7], cementation [8], electro-dialysis [9]. These methods are not economical and have many disadvantages such as incomplete metal removal, high reagent and energy consumption, and generation of toxic sludge or other waste products that require disposal or treatment. In contrast, the adsorption technique is one of the preferred methods for the removal of heavy metal ions because of its efficiency and low cost [10].

Although, previous researchers have investigated the removal of copper ions by utilizing natural clinoptilolite [11], amino-functionalized magnetic nanoparticles [12], pectin–iron oxide magnetic nano-composite [13], Carboxymethyl-cyclodextrin conjugated magnetic nanoparticles [14], polymer nano-fibrous materials [15], titanate nanotubes [16], and palm shell activated carbon [17] yet to our knowledge, sorption of copper onto nZVI has not been the subject of detailed studies. The main objective of this research is to investigate the kinetics, isotherms and thermodynamics of sorption of copper ions onto core shell zerovalent iron nanoparticle vis-à-vis the optimization of sorption physicochemical parameters (pH, contact time, initial copper ions concentration and temperature).

Materials and Methods

Synthesis of Zerovalent Iron nanoparticles

All the chemicals used are of analytical grade purchased from Sigma Aldrich, USA. The two precursors used for the synthesis of zerovalent iron nanoparticles are 0.023 M solution of Ferric Chloride and 0.125 M solution of $NaBH_4$ in the ratio 1:5 respectively following the procedure reported elsewhere in

the literature [18, 19]. For better formation of nanoscale zerovalent Iron (nZVI), more of $NaBH_4$ solution is needed than Fe^{3+} solution. As soon as the borohydride solution is added to Ferric chloride solution drop by drop in a glove box under inert environment. Ferric ion was reduced to zerovalent iron with an indication of a colour change according to the reaction:

$$4Fe^{3+} + 3BH_4^- + 9H_2O \rightarrow 4Fe^0\downarrow + 3H_2BO_3^- + 12H^+ + 6H_2\uparrow \quad (1)$$

The black particles of (nZVI) that appeared was further stirred for 3 h. nanoscale zerovalent Iron (nZVI) was separated from the solution using vacuum filtration apparatus and a cellulose nitrate membrane filter (Millipore filter) of 0.45 μm. nZVI was further washed with absolute ethanol three times and dried in a Genlab oven at 80 °C overnight.

SEM/EDX, FTIR and BET Characterization of the adsorbent:

The zerovalent iron nanoparticles were characterized by a combination of scanning electron microscopy and energy dispersive x-ray. The scanning electron microscopy (SEM) was used for the determination of the structural morphology; the quantitative elemental determination was done through the energy dispersive x-ray. The FTIR spectrum provided information about the local molecular environment on the surface of nZVI. The analysis on the determination of surface area, pore size and volume were performed using Brunauer-Emmett-Teller (BET) and Barrett-Joyner-Halenda (BJH) methods.

Sorption Experiment- Batch Sorption Studies

The batch experiment was carried out following a similar procedure reported by Adekola *et al.*2012 [20] and Dada *et al.* 2013 [21]. In a typical experiment, stock solution of 1000 ppm Cu^{2+} was prepared by dissolving a calculated amount of $CuSO_4.5H_2O$ (3.927g) in 1000 cm^3 of distilled deionized water in a standard volumetric flask and serial dilution was made to prepare 10 – 100 ppm of the adsorbate. Batch sorption of Cu^{2+} ions onto nZVI was carried out and the sorption physicochemical parameters were determined. Generally, sorption experiment was done by contacting 100 mg of the nZVI with 50 cm^3 of different initial Cu^{2+} concentrations from 10ppm – 100 ppm in 60 cm^3 of Teflon bottle intermittently for 3 hours. The mixture was filtered and the filtrate was immediately analyzed for metal ions concentration using atomic absorption spectrophotometer (AAS) model AA320N at the Department of Physical Sciences, Industrial Chemistry Unit, Landmark University. The determination of the residual concentration using AAS was done in triplicate and the mean value for each set of the experiment was calculated. Optimization of sorption parameters (pH, contact time, adsorbent dose) was investigated following a similar procedure. Adsorption capacities

were obtained using a mass balance equation [21]:

$$Q = \frac{(c_o - c_e)V}{m} \quad (2)$$

where Q is the equilibrium adsorption capacity per gram of nZVI (mg g^{-1}), V is the volume of Cu^{2+} solution (L), C_o is the initial concentration of the Cu^{2+} solution before sorption (mg L^{-1}), C_e is the final concentration of the Cu^{2+} solution after sorption (mg L^{-1}), m is the mass in gram of nZVI. The removal efficiency was calculated using the formulae in Eq. (3) as reported in the literature [22]

$$\% RE = \frac{C_i - C_e}{C_i} \times 100 \quad (3)$$

The adsorption data obtained from the optimized parameters were tested and analyzed using kinetics models (pseudo-first and pseudo-second order, Elovich, power factor and intra-particle diffusion) and six different isotherm models (Langmuir, Freundlich, Temkin, Dubinin-Raduskevich, Halsey and Harkin-Jura)

Optimization of pH, Adsorbent Dose, Contact time and Initial Cu^{2+} concentration

The effect of pH, adsorbent dose contact time, initial Cu^{2+} concentrations were investigated to determine the optimum conditions. The effect of pH on sorption of Cu^{2+} onto nZVI was done by adjusting the pH using 0.1 M HCl and 0.1 M NaOH solutions. The effect of pH on the sorption of Cu^{2+} was carried out within the pH range of 1 – 7 that will not influence Cu^{2+} precipitation [23, 24].

The effect of adsorbent dose was carried out at optimum pH, contact time and initial concentration of 100 mg L^{-1} and variable adsorbent doses of about 10 mg – 150 mg was contacted with 50 cm^3 portions of Cu^{2+} solution. The residual concentration was determined by AAS.

The effect of contact time on the sorption of Cu (II) ions onto nZVI was studied at various time intervals (0 – 120 min) at optimum pH and at different initial concentrations of 40 mgL^{-1}, 60 mgL^{-1}, 80 and 100mgL^{-1}. 100 mg adsorbent dose of nZVI was agitated with 50cm^3 of the Cu(II) solution in 60 cm^3 Teflon bottle at the optimum conditions and the residual Cu^{2+} concentration was determined in triplicate using AAS. The amount of metal ions sorbed was calculated using Eq. 2 and adsorption kinetics and mechanism were determined by data analysis using different kinetics models (pseudo first-order, pseudo second-order, Elovich, fractional power and intra-particle diffusion).

The effect of initial Cu^{2+} ions concentration on the extent of uptake was investigated as reported in the literature [25]. This was done by agitating 100 mg of nZVI added into 50 cm^3 portions of Cu^{2+} solutions within the range of 10 – 100 mgL^{-1} on the orbital shaker at optimum time of 60 minutes. The amount of metal ions sorbed was calculated and

the data were fitted into six different isotherm models such as: Langmuir, Freundlich, Temkin, Dubinin-Raduskevich (D-R), Halsey and Harkin-Jura.

Results and Discussion

Characterization of Zerovalent Iron Nanoparticles

Table 1 shows the physiochemical parameters of zerovalent iron nanoparticles. The Point of zero charge (PZC) is defined as the pH at which the surface of the adsorbent (nZVI) has a net neutral charge. The PZC of nZVI as determined by salt addition method is 5.28 (Fig not shown). The significance of this is that nZVI has a positive charge at solution pH values less than the PZC and thus a surface on which anions may adsorb. On the other hand, nZVI has a negative charge when the pH of the solution is greater than the PZC and thus be a surface on which cation may adsorb and thus the pH of nZVI is 5.28 indicating that nZVI better adsorption capacity was obtained at as solution pH greater than 5.28 stated on Table 1 [26].

The surface area by BET is 20.8643 m^2/g, the t-Plot micropore area is 4.4140 m^2/g which is lower than the t-Plot external surface area (is 16.4503 m^2/g). These results revealed that most of the Cu^{2+} ions are adsorbed at the external surface area and hence adsorption prevails. The large surface of nanoscale zerovalent iron (nZVI) enhances its relevance in the waste water remediation [27].

The SEM micrograph of ZVI showed a spherical surface of chain-like, aggregated molecules. The chain-like aggregation is an indication of its magnetic property. The EDX spectrum of nZVI (Fig 1) showed the characteristics peaks of the nZVI, the information on the surface atomic distribution and the chemical elemental composition couple with the percentage composition of the prepared are stated in Table 2. Iron (Fe) has the highest atomic weight and atomic abundance of 86.47% and 51.28% (Table 2) respectively, this is in accordance with the report of the literature [28, 29].

Figure 2 showed the FTIR spectrum of nZVI. The peaks on Fig. 2 are 3345 cm^{-1}, 3256 cm^{-1}, 1632 cm^{-1}, 1328 cm^{-1}, 910 cm^{-1}, and 686 cm^{-1}. The broad and intense peak around 3345 cm^{-1}, 3256 cm^{-1} is due to the presence of O─H from alcohol used in washing nZVI to prevent rapid corrosion. The peak at 1632 cm^{-1} may be attributed to H─O─H stretching of deionized deoxygenated water, 1328 cm^{-1} corresponds to C─H bending, 910 cm^{-1} is due to C─H bending out of plane and 686 cm^{-1} is attributed to zerovalent iron, Fe^0 as reported in the literature [28, 29, 30].

Optimization of pH, Contact time and Initial Concentration.

Effect of pH places one of the greatest roles in the adsorption studies because it influences the surface charge of the adsorbents, ionic mobility, the degree of

ionization and speciation of different pollutants and solution chemistry of contaminants (i.e. hydrolysis, redox reactions, polymerization and coordination) [26]. Fig 3 shows the plot the effect of pH on the sorption of Cu^{2+} onto nZVI. The percentage removal efficiency increases greatly from pH 4 (68.158 %) to pH 6 (86.3 %) where it attained equilibrium. The low percentage removal efficiency observed from pH 1 to 3 is a result of increase in electrostatic effect arising from the competition among Cu^{2+}, H_3O^+ and other cationic species ($Cu(OH)^+$, $Cu(OH)_2$, $Cu(OH)_3^-$ and $Cu(OH)_4^{2-}$) for adsorption sites at lower pH. As the pH of the solution increases, the competition for adsorption site reduces and more of Cu^{2+} dominates thereby leading to increase in the quantity adsorbed (34.08 mg/g – 43.15 mg/g) and considerable increase in the percentage removal efficiency. The optimum pH observed was pH 6 and all other optimization studies were carried out at this pH [12, 13, 14, 26].

The effect of adsorbent dose on the sorption of Cu^{2+} onto nZVI is shown on Fig 4. Increase in the adsorbent dose from 18.99 mg/g at 10mg to 22.62 mg/g was a result of increase in the number of active site as the adsorbent increases. This is similar to findings reported in the literature [30].

The effect of contact time (Fig 5) is another important factor in all transfer phenomena such as adsorption. A short contact time to reach equilibrium indicates the fast transport of Cu^{2+} ions from the bulk to the outer and inner surface of nZVMn. In addition, contact time also controls the buildup of charges at the solid-liquid interfaces and for this reason, optimization of the contact time on the effect of sorption of Cu^{2+} onto nZVI was investigated at three different initial concentrations 40ppm, 60ppm and 100ppm from 10min to 120min. The rate of reaction was rapid from 10 min with 16.878 mg/g, 25.854 mg/g and 40.03 mg/g (Fig 5) at the three concentrations respectively. The contact time of 60 minutes was observed as the optimum time after which a steady state approximation set in and a quasi-equilibrium situation was attained. All other optimization studies were carried out at 60 minutes contact time. Fig. 6 shows the result of the effect of initial Cu^{2+} ion concentration on the sorption of Cu^{2+} onto nZVI. As the initial concentration increased from 10ppm to 100ppm, the percentage removal efficiency also increased as a result of available and vacant active sites at low concentration and as the concentration increased, the active site became saturated and a state of equilibrium was attained where there was no significant increase in the percentage removal efficiency [25, 31]

Adsorption Kinetics

The kinetic models were exploited to test the experimental data obtained from contact times ranging from 10 to 120 minutes by monitoring the

quantity of Cu^{2+} adsorbed. In order to determine the mechanisms of sorption and its potential rate controlling steps which include mass transport and chemical reaction process, pseudo first-order, pseudo second-order, Elovich, power function (fractional power) and intraparticle diffusion rate equations have been used to model the kinetics of sorption of Cu^{2+} onto nZVI. The constant parameters, correlation coefficient ***(R^2)*** and their values are summarized on Table 3

The pseudo first-order equation (Lagergren's equation) describes adsorption in solid–liquid systems based on the sorption capacity of solids. It is assumed that one copper ion was sorbed onto one sorption site on the nZVI surface [32]:

$$S + Cu_{aq}^{2+} \xrightarrow{k_1} S.Cu_{solid-phase} \qquad (4)$$

Where S represents an unoccupied sorption site on the nZVI

The pseudo first-order equation is generally expressed as:

$$dq/dt = k_1(q_e - q_t) \qquad (5)$$

where q_e is the amount of Cu^{2+} adsorbed at equilibrium per unit weight of the adsorbent (mg/g), q_t is the amount of Cu^{2+} adsorbed at any time (mg/g) and k_1 is the pseudo first-order rate (constant/min). After the equation is integrated and boundary conditions (t =0–t and q_t =0– q_t) are applied the equation becomes:

$$Log(q_e - q_t) = Log\ q_e - \frac{k_1 t}{2.303} \qquad (6)$$

The values of $Log(q_e - q_t)$ were linearly correlated with t. The plot of $Log(q_e - q_t)$ versus t as shown on Fig. 7 gave a linear relationship and k_1 and q_e were determined from the slope and intercept of the expression in Eq. 5 respectively. The parameters are summarized on Table 3 and it showed that the kinetics model did not fit into pseudo first order model equation because the correlation coefficient was very low and the adsorption capacity calculated using this model was not close to the experimental quantity adsorbed indicating that the data were poorly fitted into pseudo first order (Hao et al., 2010)

The pseudo second-order rate expression, which has been applied for analyzing Chemisorption kinetics from liquid solutions [31, 32].

$$dq/dt = k_2(q_e - q_t)^2 \qquad (7).$$

where k_2 is the rate constant of for pseudo second-order adsorption equation (g/mg min). For the boundary conditions (t =0– t and q_t =0– q_t), the integrated form of Eq. (6) is linearly expressed as:

$$\frac{t}{q_t} = \frac{1}{k_2 q_e^2} + \frac{1}{q_e} t \qquad (8)$$

$$h_0 = k_2 q_e^2 \qquad (9)$$

Substituting h_o into equation above, it becomes:

$$\frac{t}{q_t} = \frac{1}{h_0} + \frac{1}{q_e} t \qquad (10)$$

where h_o is the initial adsorption rate. The plot of t/q_t against t as shown on

Fig. 8 gave a linear plot with good and commendable correlation coefficients close to unity at each concentration as shown on Table 3. The pseudo second-order parameters, k_2, q_e and h_o were determined from the slope and intercept of Eq. 10

When *t* tends to 0, h_o is defined as:

$$h_0 = k_2 q_e^2 \qquad (11)$$

This model assumes that one copper ion is sorbed onto two sorption sites on the nZVI surface:

$$2S + Cu_{aq}^{2+} \xrightarrow{k_1} S_2.Cu_{solid-phase} \qquad (12)$$

From the parameters summarized on Table 3, the adsorption kinetics can be best described by pseudo second-order model. The R^2 values at each concentration are greater than 0.99 and the calculated quantity adsorbed was perfectly close to experimental quantity adsorbed. This is in accordance with the findings reported in the literature [18, 32, 33, 34]

The Elovich model is generally described as:

$$dq/dt = \alpha \exp(-\beta q_t) \qquad (13)$$

Applying the boundary conditions (q_t=0 at t = 0 and $q_t = q_t$ at t = t), the simplified form of the Elovich equation is expressed as [35]:

$$q_t = \frac{1}{\beta}\ell n\left(\frac{\alpha}{\beta}\right) + \frac{1}{\beta}\ell n(t) \qquad (14)$$

where q_t is the amount of adsorbate per unit mass of sorbent at time (t). The initial adsorption rate, $\propto$ (mg/g-min) and the desorption constant (β) (g/mg) during any experiment were determined from the slope(1/β) and intercept (1/β)ln($\propto$/β) of linear plot of q_t versus (t) as shown on Fig. 9. From the parameters on Table 3, it can be deduced that since the values of R^2 were to unity and the adsorption rates were also high, the data could also be described by the Elovich model.

The Fractional power model can be expressed as [20,31]:

$$q_t = kt^{v} \qquad (15)$$

The equation above is linearized as:

$$\ell og\ (q_t) = \log(k) + v\log(t) \qquad (16)$$

where q_t is the amount of sorbate per unit mass of sorbent, k is the fractional power rate constant, t is time, and v is a positive constant (<1). The parameters v and k were determined from slope and intercept of a linear plot of log (q_t) versus log (t) as shown on Fig. 10. The parameters shown on Table 3 indicated that the parameter fit also into the fractional model because the values of v were less than 1 and the regression coefficient (R^2) was greater than 0.96 at optimum concentration [30]

The intra particle diffusion equation as expressed by Weber-Morris is given as [35]:

$$q_t = k_{id}t^{0.5} + C \qquad (17)$$

Where k_1 is the intra particle diffusion rate constant (mg $g^{-1}min^{1/2}$) and C is the intercept determined from the linear plot of q_t versus $t^{0.5}$ (Fig. 11). The intercept of the plot reflects the boundary layer effect. Higher values of the boundary layer effect obtained (16.246, 25.628

and 39.667) are indication greater contribution of the surface sorption in the rate controlling step. The calculated intra particle diffusion coefficient (k_{id}) values are listed in Table 3. Since the linear plot of q_t versus $t^{1/2}$ did not pass through the origin, then intra particle diffusion not the sole rate-limiting step [36].

Adsorption Isotherms

The adsorption isotherm constant parameters, correlation coefficient (R^2**)** and their values are summarized in Table 4.

Langmuir Adsorption Isotherm assumes a monolayer adsorption onto a homogeneous surface with a finite number of identical sites also there is uniform energy of adsorption onto the surface and no transmigration of adsorbate in the plane of the surface [37, 38]. The linear form of Langmuir represents:

$$\frac{Ce}{Q_e} = \frac{1}{K_L Q_{\max}} + \frac{C_e}{Q_{\max}} \qquad (18)$$

$Q_{\max}$ is the maximum monolayer coverage capacity ($mg.g^{-1}$), K_L is the Langmuir isotherm constant ($L.mg^{-1}$) related to the energy of adsorption. The essential features of the Langmuir isotherm may be expressed in terms of equilibrium parameter R_L, which is a dimensionless constant referred to as separation factor or equilibrium parameter [38].

$$R_L = \frac{1}{1 + K_L C_o} \qquad (19)$$

Figure 12 shows the Langmuir isotherm model plot for sorption of Cu^{2+} onto nZVI. The Langmuir contants, $Q_{\max}$ and K_L were determined from the linear plot of Ce/Qe versus Ce as shown on Fig 12. The value of separation factor, R_L (Fig 13) indicates the adsorption nature to either unfavourable or favourable. If R_L>1, it is unfavorable, linear if R_L=1, favorable if 0< R_L <1 and irreversible if R_L = 0. Since the value of separation factor (R_L) ranges from 0.110 at 10ppm to 0.021 at 100ppm and none of them was greater than 1 therefore, the adsorption of Cu^{2+} onto nZVI was favourable. In addition, the regression coefficient (R^2>0.90) and maximum monolayer coverage capacity ($Q_{\max}$ = 40.816 mg/g) revealed that the equilibrium sorption can be best described by Langmuir model which supported a chemisorption mechanism

The Freundlich sorption isotherm gives an expression encompassing the surface heterogeneity and the exponential distribution of active sites and their energies. The Linear form of Freundlich equation is [36, 37:

$$\log Q_e = \log K_f + \frac{1}{n} \log C_e \qquad \textbf{(20)}$$

The Freundlich isotherm constants, K_f and n are parameters characteristic of the sorbent-sorbate system, which were determined from the intercept and slope of the plot of $LogQ_e$ against $LogC_e$ (Fig 14) from the Table 4, the value of n (2.853) less than 10 is also an indication of a favourable adsorption. However, the

sorption data could not be best described by Freundlich model compared to Langmuir model.

Temkin Isotherm contains a factor that explicitly taking into the account of adsorbent–adsorbate interactions in a chemisorption mechanism. The model assumes that heat of adsorption (function of temperature) of all molecules in the layer would decrease linearly with the surface coverage due to adsorbent–adsorbate interactions. The linear form of the equation is given as [39]:

$$Q_e = \frac{RT}{b_T} \ln A_T + \frac{RT}{b_T} \ln Ce . \qquad (21)$$

Where B=RT/b_T, $\boldsymbol{b_T}$ is the Temkin isotherm constant related to the heat of sorption and A_T is the Temkin isotherm equilibrium binding constant (Lg^{-1}). The values of theses constants were determined from the slope and intercept obtained from appropriate plot of Q_e versus *lnCe* as shown in figure 15 and are clearly shown on Table 4. The high value of coefficient of regression (R^2 = 0.937) obtained from Temkin model corroborated the chemisorption mechanism as inferred from Langmuir Model.

Dubinin–Radushkevich (D-R) isotherm model is generally applied to express the adsorption mechanism with a Gaussian energy distribution onto a heterogeneous surface. The model has often successfully fitted high solute activities and the intermediate range of concentrations data well. The linear equation is given by [36, 37, 38, 39]:

$$\ell n Q_e = \ell n Q_d - A_{D-R} \varepsilon^2 \qquad (22)$$

Where $A_{D\text{-}R}$ is the DRK isotherm constant (mol^2/kJ^2) related to free sorption energy and Q_d is the theoretical isotherm saturation capacity (mg/g). The values of $A_{D\text{-}R}$ and Q_d were determined respectively from the slope and intercept of the plot of *ln Qe versus* ε^2 (Fig 16). The parameter ε is the Polanyi potential which is computed as:

$$\varepsilon = RT \ell n \left[1 + \frac{1}{C_e} \right] \qquad (23)$$

The approach was usually applied to distinguish the physical and chemical adsorption of metal ions with its mean sorption free energy, E per molecule of adsorbate (for removing a molecule from its location in the sorption space to the infinity) can be computed by the relationship [40]:

$$E = -\left[\frac{1}{\sqrt{2A_{D-R}}} \right] \qquad (24)$$

If the value of mean sorption free energy (E) is less than 8kJ mol^{-1}, the adsorption mechanism will be physisorption and if the value of E is greater than 8kJ mol^{-1}, the adsorption will be chemisorption. Since the magnitude of E (free energy of transfer of one solute from infinity to the surface of nZVI) is greater than 8KJ mol^{-1} (Table 4), the adsorption mechanism is chemisorption which further supported Langmuir Isotherm [39].

Both Halsey isotherm and Harkin-Jura are used to evaluate the

multilayer adsorption at a relatively large distance from the surface. The Halsey isotherm is expressed by [36, 39]:

$$\ell nq_e = \left[\left(\frac{1}{n_H}\right)\ell nK\right] - \left(\frac{1}{n_H}\right)\ell nC_e \quad (25)$$

A plot of ℓnq_e against ℓnC_e gave a linear graph (Fig 17) and the Halsey constants K_H and n_H were determined from the intercepts and slope respectively. The Halsey isotherm model is always in support of Freundlich model and an evidence of this is shown from the regression coefficient (R^2 = 0.874) which is similar to that obtained from Freundlich model. Both Freundlich and Halsey models always support multilayer adsorption [39]. A low regression coefficient obtained from both Freundlich and Hasley models is an indication that the equilibrium data did not follow multilayer adsorption.

The Harkin-Jura isotherm is expressed as:

$$\frac{1}{q_e^2} = \frac{B_{HJ}}{A_{HJ}} - \frac{1}{A_{HJ}}\ell ogCe \quad (26)$$

The Harkin-Jura constants A_{HJ} and B_{HJ} were determined from the slope and intercept of the linear plot of $\frac{1}{q_e^2}$ versus $\ell ogCe$ as shown on figure 18. The parameters of Harkin-Jura isotherm model are as shown on Table 4 revealed that the equilibrium sorption data is poorly described by this model which further supported chemisorption process.

Thermodynamic studies

Temperature is another important parameter in the adsorption studies because some important parameters like enthalpy change (ΔH), entropy change (ΔS) and Gibbs free energy change (ΔG) could be determined. The thermodynamic parameters can be determined from the thermodynamic equilibrium constant, K_a (or the thermodynamic distribution coefficient). The standard Gibbs free energy ΔG^o (kJ mol^{-1}), standard enthalpy change ΔH^o (kJ mol^{-1}), and standard entropy change ΔS^o (J $mol^{-1}K^{-}1$) were calculated using the following equations [30, 40]:

$$Ka = \frac{q_e}{Ce} \quad (27)$$

$$\Delta G = -RT\ell nKa \quad (28)$$

$$LogKa = \frac{\Delta S}{2.303R} - \frac{\Delta H}{2.303RT} \quad (29)$$

The Van't Hoff plot on sorption of Cu^{2+} onto nZVI is shown on Fig. 19 and the thermodynamic parameters are stated on Table 5. The positive standard enthalpy change (ΔH^o = 53.44925 $kJmol^{-1}$) for this study suggests that the adsorption of Cu^{2+} by nZVI is endothermic in nature, which is supported by the increase in Cu^{2+} adsorption with increase in temperature from 298 K to 318 K. The positive standard entropy change (ΔS^o = 45.3Jmol−1 K−1) reflected the affinity of the nZVI particles towards Cu^{2+} and the negative values of the standard Gibbs free energy ΔG^o (Table 5) is an indication of the

feasibility and spontaneity of the adsorption process.

Conclusion

The synthesis of nanoscale zerovalent iron via single pot system vis-à-vis chemical reduction is a novel approach. The isotherms, kinetics and thermodynamic studies of sorption of Cu^{2+} onto zerovalent iron nanoparticles was investigated. Optimization studies revealed that pH, contact time, initial concentration, adsorbent dose and temperature played substantial role in adsorption studies and maximum adsorption capacity can be obtained at pH 6 for sorption of Cu^{2+}. The pseudo first-order, pseudo second-order, Elovich, power function (fractional power) and intra particle diffusion rate equations have been used to model the kinetics of sorption of Cu^{2+} and from this investigation, pseudo second-order best described the kinetic process. From the six different adsorption isotherm models investigated, equilibrium sorption data fitted best into Langmiur and Temkin isotherm models indicating a Chemisorption mechanism and this was also supported with the high energy value calculated from DRK isotherm model which is in the range of the energy values for Chemisorption process. The values obtained from the thermodynamic parameters, ΔH, ΔS, and ΔG vividly proved the reaction was feasible, spontaneous and endothermic in nature. Outcome of this research showed that zerovalent iron nanoparticle is an effective and promising nano-adsorbent for the sorption of toxic heavy metal ions.

Acknowledgement

Dada, Adewumi Oluwasogo wishes to appreciate the management of Landmark University for providing enabling environment and facilities for novel, result oriented research and opportunity to carry out my Ph.D. programme in University of Ilorin,

References

Brewer, G.J. (2010). Copper toxicity in the general population. *Clin Neurophysiol*. 121(4):459-60. doi:10.1016/j.clinph.2009.12.015 PMID 20071223

Casarett and Doull's Toxicology, The Basic Science of Poisons, Fifth Edition, Edited by Curtis D. Klassen, Ph.D., McGraw-Hill, New York. pp 715.

Kardiravela, K and Namsasivayan, C. (2003). "Activated carbon from coconut coir- pith as metal adsorbent: adsorption of Cd (II) aqueous solution" . *Advances in Environmental Researcher 411 – 418.*

Richard, A.L and Tay O.C (1980) *Encyclopedia Americana*, pp 137 – 139.

Yoon, Y., Amy, G. and Yoon, J. (2005). ''Effect of pH and conductivity on hindered diffusion of per chlorate ions during transport through negatively charged nanofiltration and ultra-filtration

membranes''. *Desalination* **177**: 217-227

Crittenden, J., Trusell, R., Hand, D., Howe, K., and Techobanoglous, G. (2005). Water treatment principle and design, 2nd Edition John Wiley & Sons. New Jersey.

Ku, Y., Wu, M-H., and Shen Y-S., (2002). ''A study on the cadmium removal from aqueous solutions by zinc cementation''. *Separation Science and Technol*., **37** (3): 571-590.

Singh, K. K., Talat, M., and Hasan, S. H., (2006) Removal of lead from aqueous solutions by agricultural waste maize bran''. *Bioresource Technol*., **97** (16): 2124-2130

Elizabeth de Olivera, Maria, J. and Santos, Y. (2003), 'Heavy metals removal in industrial Efficient by sequential adsorbent treatment', *Advancement in Environmental Research. 7(2): 263 – 272.*

Kamimura, Y., Chiba, H., and Utsumi, H (2002). "Barrier function of micro vessels and roles of glial cell line-derived neurotrophic factor in the rat testis," *Medical Electron Microscopy*, Vol.35, pp. 139–145.

Jovanovic, M., Rajic, N., and Obradovic, B. (2012). Novel kinetic model of the removal of divalent heavy metal ions from aqueous solutions by natural clinoptilolite, *Journal of Hazardous Materials* **233–234**: 57– 64

Hao Y-M., Chen, M., Hu, Z-B (2010). Effective removal of Cu (II) ions from aqueous solution by amino-functionalized magnetic nanoparticles, *Journal of Hazardous Materials* **184**: 392–399

Gong, J-L., Wang, X-Y., Zeng, G-M., Chen, L., Deng, J-H., Zhang, X-R., Ni, Q-Y. (2012). Copper (II) removal by pectin–iron oxide magnetic nanocomposite adsorbent. *Chemical Engineering Journal* **185–186**: 100 – 107

Badruddoza, A.Z.M., Tay, A.S.H., Tan, P.Y., Hidajat, K., Uddin, M.S (2011) Carboxymethyl- -cyclodextrin conjugated magnetic nanoparticles as nano-adsorbents for removal of copper ions: Synthesis and adsorption studies, *Journal of Hazardous Materials* **185:** 1177–1186

Xiao, S., Ma, H., Shen, M., Wang, S., Huang, Q., Shi, X. (2011). Excellent copper (II) removal using zerovalent iron nanoparticle-immobilized hybrid electrospun polymer nano-fibrous materials, *Colloids and Surfaces A: Physicochemical. Eng. Aspects* **381**: 48–54

Liu, W., Ting Wang, T., Borthwick, A.G.L., Wang, Y., Yin, X., Li, X., Ni, J. (2013) Adsorption of Pb^{2+}, Cd^{2+}, Cu^{2+} and Cr^{3+} onto titanate nanotubes: Competition

and effect of inorganic ions. *Science of the Total Environment* **456–457**: 171–180

Onundi, Y.B., Mamun, A.A., Al Khatib, M.F. and Ahmed, Y.M (2010). Adsorption of copper, nickel and lead ions from synthetic semiconductor industrial wastewater by palm shell activated carbon *International Journal of Environ. Sci. Tech.,* **7**(4): 751-758.

Boparai, H.K., Meera, J., Dennis, M.O. (2010) Kinetics and thermodynamics of Cadmium ion removal by adsorption onto nano zervalent iron particles. *Journal of Harzard. Mater, Doi:10.1016/j.jhazmat.2010.11. 0 29*

Dada, A.O., Adekola, F.A and Odebunmi, E.O (2014). Investigation of the Synthesis and Characterization of Manganese Nanoparticles and its Ash Rice Husk Supported Nanocomposite, *Book of Proceedings of 1st African International Conference/Workshop on Applications of Nanotechnology to Energy, Health and Environment – March 23rd – 29th, 2014*. pg 62.

Adekola, F.A., Abdu's Salam, N., Adegoke, H.I., Adekola, A.M., and Adekeye, J.I.D (2012) Removal of Pb (II) from aqueous solution by natural and synthetic calcites. *Bulletin Chemical Soc. Ethiop*. **26** (2): 195-210.

Dada, A.O., Ojediran, J.O., and Olalekan, A.P., (2013). Sorption of Pb^{2+} from Aqueous Solution unto Modified Rice Husk: Isotherms Studies. *Advances in Physical Chemistry,http://dx.doi.org/10.1155 /2013/842425*

Vasuderan, P., Padmavathy, V., Dhingra, S.C. (2003). ''Kinetics of biosorption of Cadmium on Baker's yeast''. *Bioresources. Technology*. ***89****(3):28-287*

Xu, H., Liu, Y., Tay, J. (2006). ''Effect of pH on nickel biosorption by aerobic granular sludge''. *Bioresources Technology*. **97**(3): 359-363.

Igwe, J.C., Abia, A.A., Ibeh, C.A., 2005. Adsorption kinetics and intraparticulate diffusivities of Hg, As and Pb ions on unmodified and thiolated coconut fiber. *International Journal of Environ. Sci. Technol*. **5**: 83–92 .

Srivastava, V. C., Mall, I. D., Mishra, I.M. (2005). ''Characterization of mesoporous rice husk ash (RHA) and adsorption kinetics of metal ions from aqueous solution onto RHA''. *Journal of hazardous material, doi:10.1016/j.jhazmat.11.052***.**

Chen, L., Sun, L.J., Luan, F., Liang, Y., Li, Y., Liu, X.X. (2010). Synthesis and pseudo capacitive studies of composite films of polyaniline and manganese

oxide nanoparticles. *Journal of Power Sources*, **195**: 3742–3747

Shahwan, T., Sirriah, A.S.; Nairat, M.; Boyacı, E.; Eroglu, A.E.; Scott, T.B.; Hallam. K.R. (2011). Green synthesis of iron nanoparticles and their application as a Fenton-like catalyst for the degradation of aqueous cationic and anionic dyes, *Chemical Engineering Journal*, **172**: 258– 266

Prema, P., Thangapandian, S., Selvarani, M., Subharanjani, S., C. Amutha (2011) Color removal efficiency of dyes using nano zerovalent iron treatment. *Toxicological & Environmental Chemistry*, **93**:10, 1908-1917

Frost, R.L., Xi, Y., He, H. (2010). Synthesis, characterization of palygorskite supported zerovalent iron and its application for methylene blue adsorption, *Journal of Colloid and Interface Science* **341**: 153–161

Ayanda, O.S., Fatoki, S.O., Adekola, F.A and Ximba, B.J. (2013) Kinetics and equilibrium models of the sorption of tributyltin to nZnO, activated carbon and nZnO/activated carbon composite in artificial seawater. *Marine Pollution Bulletin.*, http: //dx.doi.org/10.1016/j.marpolbul .2013.04.001

Ho, Y.S. (2004) Citation review of Lagergren kinetic rate equation on adsorption reactions, *Scientometrics*, **59**:171–177.

Ho, Y.S. (2006) Review of second-order models for adsorption systems, *Journal of Hazardious Material*. **136**: 681–689.

Azizian, S. (2004) Kinetic models of sorption: a theoretical analysis, *Journal of Colloid Interface Sci*. **276**: 47–52.

Hameed, B.H, D.K. Mahmoud, D.K. A.L. Ahmad, A.L. (2008) Equilibrium modeling and kinetic studies on the adsorption of basic dye by a low-cost adsorbent: Coconut (*Cocos nucifera*) bunch waste, *Journal of Hazardous Materials* **158**: 65–72

Igwe, J. C. and Abia A.A. (2006) A bioseparation process for removing heavy metals from waste water using biosorbents, *African Journal of Biotechnology* **5** (12), pp. 1167-1179

Bhatt, R.R., Shah, B.A. (2013). Sorption studies of heavy metal ions by salicylic acid–formaldehyde–catechol terpolymeric resin: Isotherm, kinetic and thermodynamic cs. *Arabian Journal of Chemistry*, http://dx.doi.o rg/10.1016/j.arabjc.2013.0 3.012

Foo, K.Y and Hameed, B.H (2010) Insights into the modeling of adsorption isotherm systems. *Chemical Engineering Journal*, **156**: 2–10

Argun, M.E., Dursun, S., Ozdemir, C. and Karatas, M. (2007) Heavy metal adsorption by modified oak sawdust:

Thermodynamics and kinetics. *Journal of Hazardous Materials*, **141**: 77–85

Chengwen, S., Shuaihua, W., Murong, C., Tao, P., Mihua, S and Guangrui, G. (2014). Adsorption Studies of Coconut Shell Carbons Prepared by KOH Activation for Removal of Lead(II) From Aqueous Solutions *Sustainability*, **6**: 86-98; doi:10.3390/su6010086

Ahmad, M.A., Ahmad, N., and Bello, O.S (2014): Removal of Remazol Brilliant Blue Reactive Dye From Aqueous Solutions Using Watermelon Rinds as Adsorbent, *Journal of Dispersion Science and Technology* http://dx.doi.org/10.1080/01932691.2014.925400

List of Figures and Tables

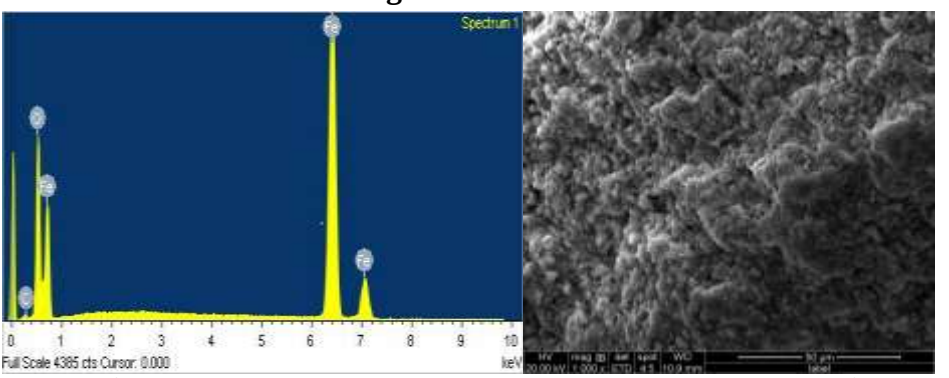

Fig 1: EDX spectrum for nZVI SEM micrograph for nZVI

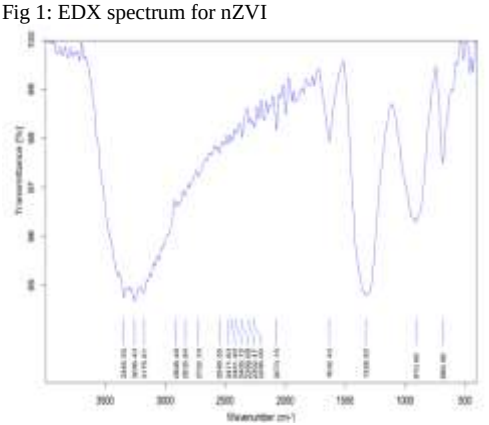

Fig 2: FTIRspectrum for nZVI

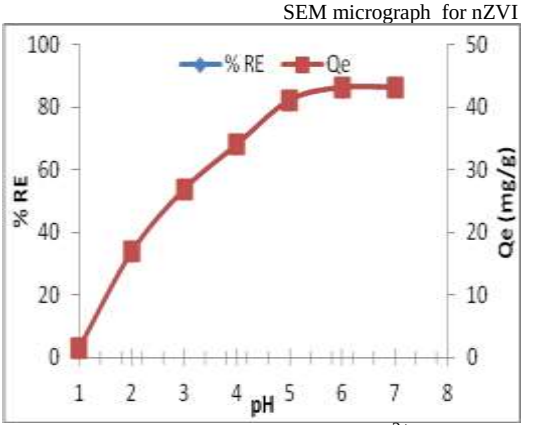

Fig 3: Effect of pH on sorption of Cu^{2+} onto nZVI

Experimental conditions: Cu^{2+} Concentration = 100 mg/L Volume of Cu^{2+} solution = 50 mL; Contact time = 60 min, Stirring speed = 200 rpm, Adsorbent Dose =100 mg and Temperature = 25± 2 ^0C

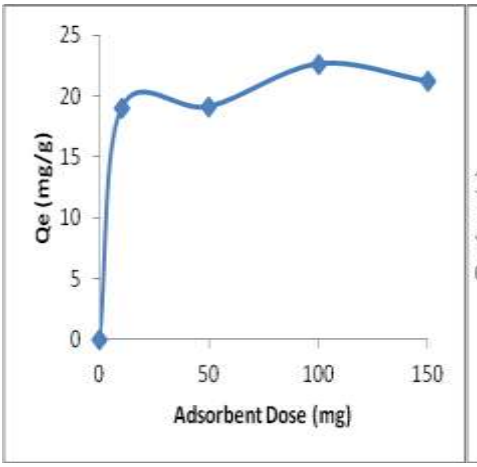

Fig 4: Effect of Adsorbent dose on sorption of Cu^{2+} onto nZVI
Experimental conditions: Cu^{2+} Concentration= 100 mg/L Volume of Cu^{2+} solution = 50 mL; pH = 6, stirring speed = 200 rpm, Contact time = 60 min, and temperature = 25± 2 ^{0}C

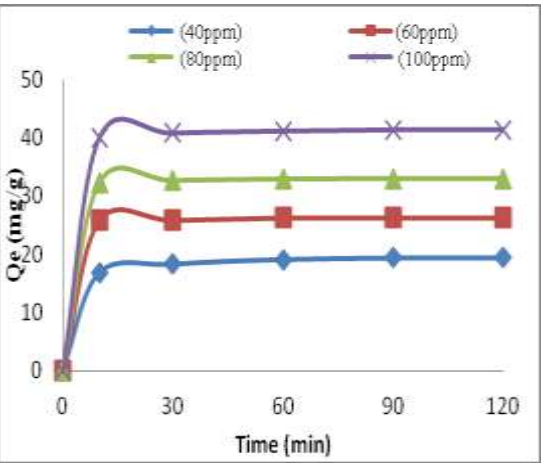

Fig 5: Effect of Contact time on sorption of Cu^{2+} onto nZVI
Experimental conditions: Cu^{2+} Concentration= 100 mg/L Volume of Cu^{2+} solution = 50 mL; pH = 6, stirring speed = 200 Adsorbent Dose =100 mg and temperature = 25± 2 ^{0}C

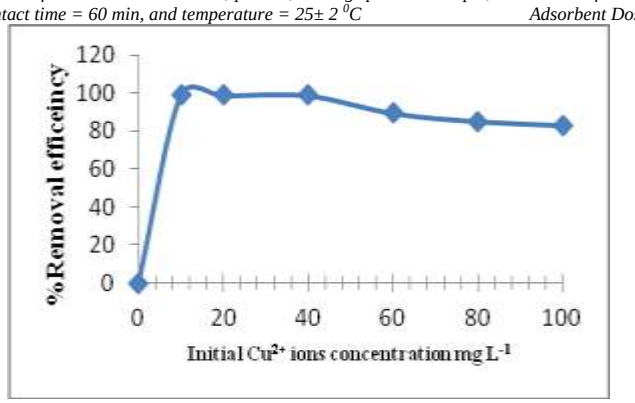

Fig 6: Effect of Initial Concentrations
Experimental conditions: Volume of Cu^{2+} solution = 50 mL; Contact time = 60 min, pH = 6; Stirring speed = 200 rpm; Adsorbent Dose =100 mg and Temperature = 25± 2 ^{0}C

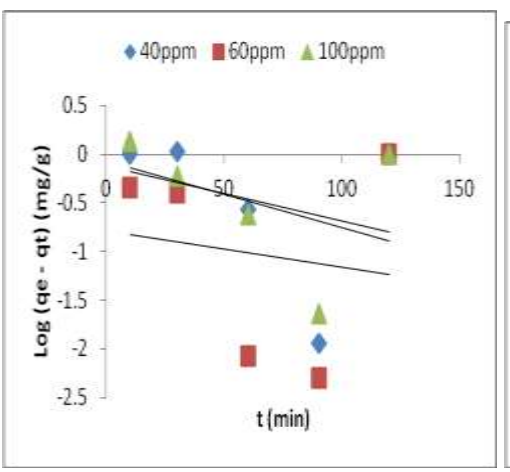

Fig 7: Pseudo first-order kinetic of sorption of Cu^{2+} onto nZVI

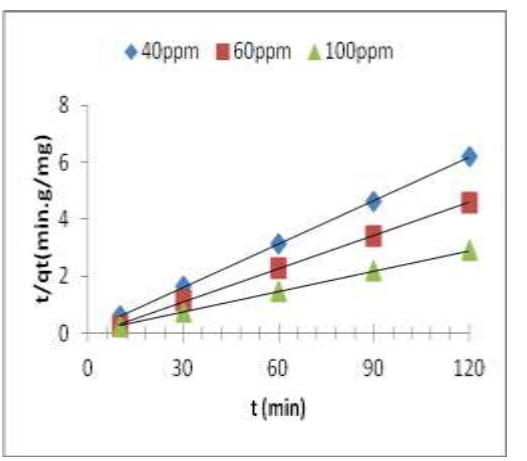

Fig 8: Pseudo second-order kinetic of sorption of Cu^{2+} onto nZVI

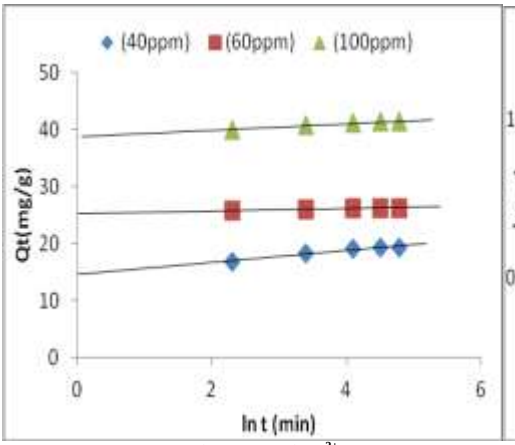

Fig 9: Elovich model of sorption of Cu^{2+} onto nZVI

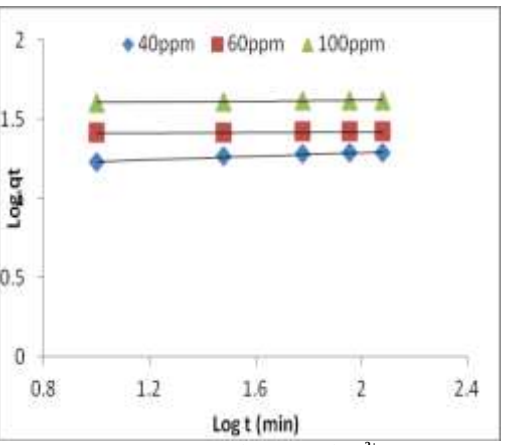

Fig 10: Fractional power of sorption of Cu^{2+} onto nZVI

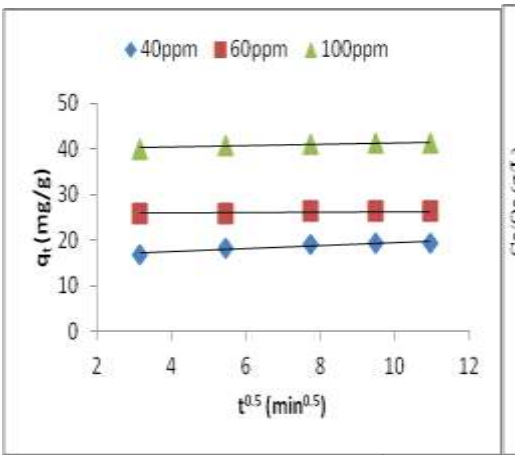

Fig 11: Intraparticle diffusion plot for sorption of Cu^{2+} onto nZVI

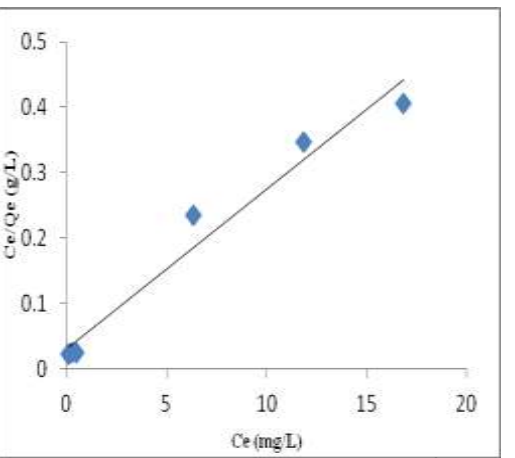

Fig 12: Langmuir Isotherm model for sorption of Cu^{2+} onto nZVI

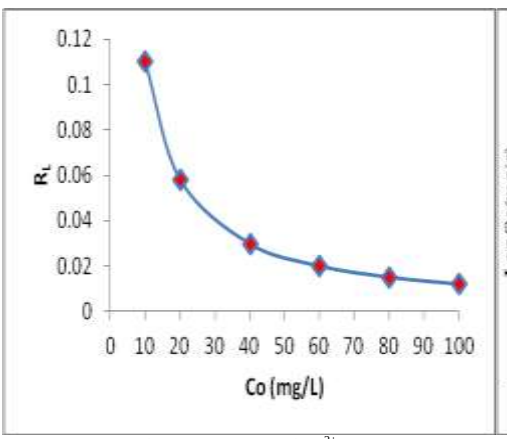

Fig 13: Separation factor on sorption of Cu^{2+} onto nZVI

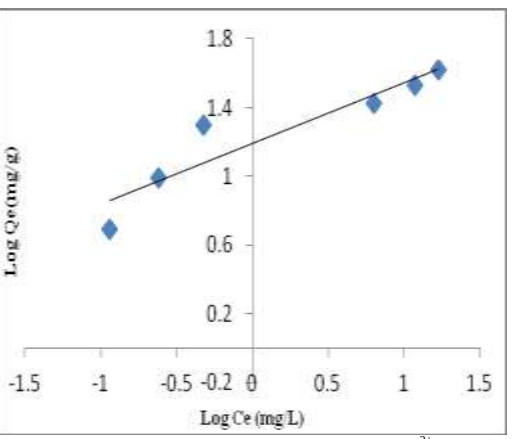

Fig 14: Freundlich Isotherm model for sorption of Cu^{2+} onto nZVI

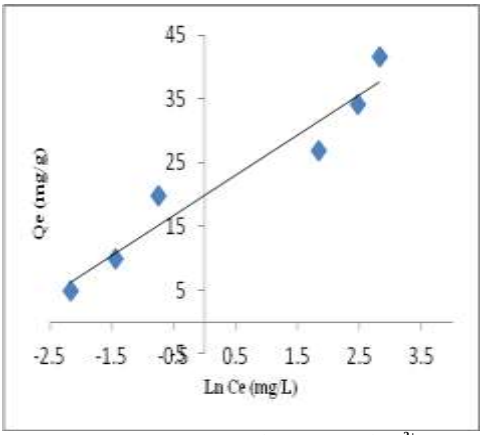

Fig 15: Temkin Isotherm model for sorption of Cu^{2+} onto nZVI

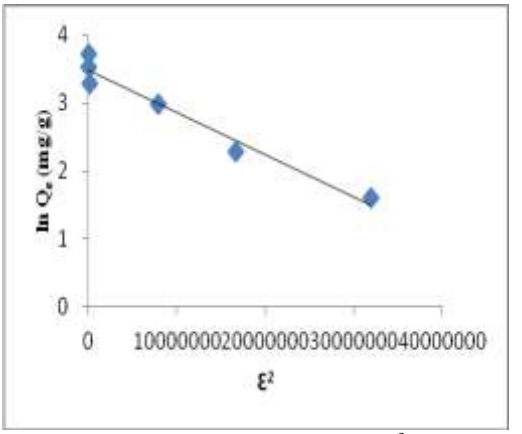

Fig 16: DRK Isotherm model for sorption of Cu^{2+} onto nZVI

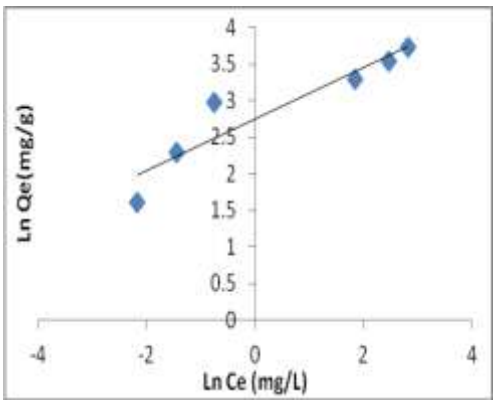

Fig 17: Halsey Isotherm model for sorption of Cu^{2+} onto nZVI

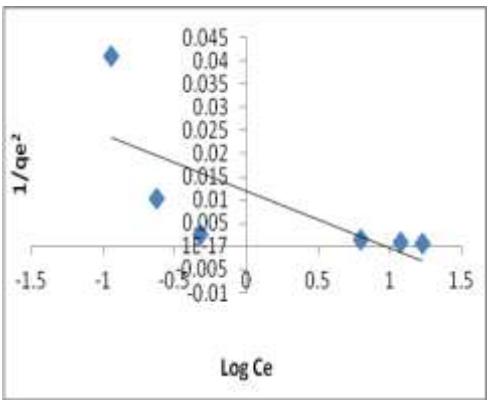

Fig 18: Harkins-Jura Isotherm model for sorption of Cu^{2+} onto nZVI

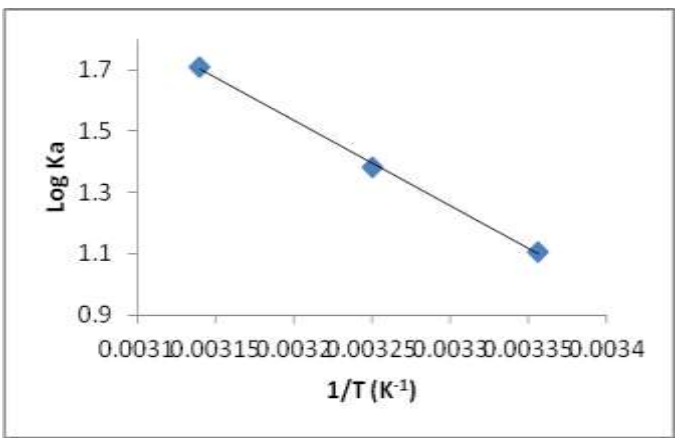

Fig 19:Van't Hoff plot on sorption of Cu^{2+} onto nZVI

Table 1: Physicochemical parameters of nZVI as adsorbent for the sorption of Cu^{2+}

pH	6.00
PZC	5.20
BET Surface Area:	20.8643 m^2/g
t-Plot Micropore Area:	4.4140 m^2/g
t-Plot External Surface Area:	16.4503 m^2/g
BJH Adsorption cumulative surface area of pores between 17.000 Å and 3000.000 Å diameter:	19.120 m^2/g
Pore Volume	
Single point adsorption total pore volume of pores less than 1070.322 Å diameter at P/Po = 0.981571614:	0.097502 cm^3/g
t-Plot micropore volume:	0.001895 cm^3/g
BJH Adsorption cumulative volume of pores between 17.000 Å and 3000.000 Å diameter:	0.115083 cm^3/g
Pore Size	
Adsorption average pore width (4V/A by BET):	186.9268 Å
BJH Adsorption average pore diameter (4V/A):	240.753 Å

Table 2: EDX Elemental percentage composition of NZVI

Element	Weight%	Atomic%
C K	1.72	4.75
O K	21.24	43.97
Fe K	86.47	51.28
Totals	109.43	100

Table 3: Kinetic model parameters for Cu^{2+} adsorption onto nZVI investigated at different concentrations

Models	40ppm	60ppm	100ppm
Pseudo first-order			
k_1	0.0159	0.00875	0.0131
qe,exp	19.388	26.305	41.39
qe,cal	0.855	0.163	0.763
R^2	0.131	0.0242	24
Pseudo second-order			
k_2	0.0264	0.1177	0.0538
qe,exp	19.388	26.305	41.39
qe,cal	19.723	25.773	41.49
H_0	10.256	13.928	92.593
R^2	1	0.999	1
Elovich			
α	$10.09x10^5$	48.196	3.932
β	0.944	4.673	1.771
R^2	0.968	0.837	0.982
Fractional Power			
K	14.887	25.322	38.833
V	0.0583	0.0082	0.0139
R^2	0.963	0.837	0.981
Intra-particle Diffusion			
K	0.0322	0.0683	0.1735
C	16.246	25.628	39.667
R^2	0.881	0.835	0.909

Table 4: Langmuir, Freundlich, Temkin, and D–R, Halsey and Harkin-Jura isotherm models parameters and correlation coefficients for adsorption of copper ions onto nZVI particles

Isotherm Models	Parameters	Cu^{2+}
Langmuir	q_{max} (mgg^{-1})	40.816
	K_L *(Lmg-1)*	0.806
	R_L	0.012
	R^2	0.966
Freundlich	k_f	15.488
	1/n	0.351
	n	2.853
	R^2	0.874
Temkin	b_T $(J\ mol^{-1})$	4.501×10^{-8}
	B (Lg^{-1})	6.2863
	A_T (Lg^{-1})	4.501×10^{8}
	R^2	0.937
DRK	q_d	32.769
	A_{DRK}	-6.008
	*E(*KJ/mol)	9.128
	R^2	0.961
Halsey	*1/n*	0.3505
	N	2.853
	K	2484.157
	R^2	0.874
Harkin-Jura	*A*	81.3008
	B	0.9675
	R^2	0.533

Table 5: Thermodynamic parameters for adsorption of Cu^{2+} onto nZVI

T (K)	ΔG(kJ mol^{-1})	ΔH (kJ mol^{-1})	ΔS (J mol^{-1} K^{-1})	Ka
298	-6.31409	53.44925	200.4323	12.782
308	-8.146.56			24.065
318	-10.4076			51.204